The Journal of Neuroscience

https://jneurosci.msubmit.net

JN-RM-0821-21R1

Identification of BiP as a CB1 receptor-interacting protein that fine-tunes cannabinoid signaling in the mouse brain

Manuel Guzman, Complutense University
Carlos Costas-Insua, Complutense University
Estefania Moreno, University of Barcelona
Irene Maroto, Complutense University
Andrea Ruiz-Calvo, Complutense University Madrid
Raquel Bajo-Grañeras, Complutense University
David Martín-Gutiérrez, Complutense University
Rebeca Diez-Alarcia, University of the Basque Country
M. Teresa Vilaró, Instituto de Investigaciones Biomédicas de Barcelona, CSIC (IDIBAPS)
Roser Cortés, Instituto de Investigaciones Biomédicas de Barcelona, CSIC (IDIBAPS)
Nuria García-Font, Complutense University
Ricardo Martín, Universidad Complutense de Madrid
Marc Espina, University of Barcelona
Joaquín Botta, Queen Mary University of London
Silvia Gines, University of Barcelona
Peter McCormick, Queen Mary University of London
Jose Sanchez-Prieto, Universidad Complutense
Ismael Galve-Roperh, Complutense University
Guadalupe Mengod, Instituto de Investigaciones Biomédicas de Barcelona, CSIC (IDIBAPS)
Leyre Urigüen, University of the Basque Country

Giovanni Marsicano, INSERM University of Bordeaux
Luigi Bellocchio, Complutense University Madrid
Enric Canela, University of Barcelona
Vicent Casadó, Universitat de Barcelona
Ignacio Rodríguez-Crespo, Complutense University

Commercial Interest:

Identification of BiP as a CB_1 receptor-interacting protein that fine-tunes cannabinoid signaling in the mouse brain

Abbreviated title: BiP interacts with cannabinoid CB_1 receptor

Carlos Costas-Insua[1,2,3], Estefanía Moreno[4], Irene B. Maroto[1,2,3], Andrea Ruiz-Calvo[1,2,3], Raquel Bajo-Grañeras[1,2,3], David Martín-Gutiérrez[2], Rebeca Diez-Alarcia[5,6], M. Teresa Vilaró[1,7,8], Roser Cortés[1,7,8], Nuria García-Font[2,9], Ricardo Martín[2,9], Marc Espina[1,7,10], Joaquín Botta[11], Silvia Ginés[1,7,10], Peter J. McCormick[11], José Sánchez-Prieto[2,9], Ismael Galve-Roperh[1,2,3], Guadalupe Mengod[1,7,8], Leyre Urigüen[5,6], Giovanni Marsicano[12], Luigi Bellocchio[12], Enric I. Canela[1,4], Vicent Casadó[4], Ignacio Rodríguez-Crespo[1,2,3,*], Manuel Guzmán[1,2,3,*]

[1]Centro de Investigación Biomédica en Red sobre Enfermedades Neurodegenerativas (CIBERNED), Madrid 28031, Spain

[2]Department of Biochemistry and Molecular Biology, Instituto Universitario de Investigación Neuroquímica (IUIN), Complutense University, Madrid 28040, Spain

[3]Instituto Ramón y Cajal de Investigación Sanitaria (IRYCIS), Madrid 28034, Spain

[4]Department of Biochemistry and Molecular Biomedicine, Faculty of Biology, Institute of Biomedicine of the University of Barcelona, University of Barcelona, Barcelona 08028, Spain

[5]Department of Pharmacology, University of the Basque Country/Euskal Herriko Unibertsitatea, Leioa 48940, Spain

[6]Centro de Investigación Biomédica en Red de Salud Mental (CIBERSAM), Madrid 28029, Spain

[7]Institut d'Investigacions Biomèdiques August Pi i Sunyer (IDIBAPS), Barcelona 08036, Spain

[8]Department of Neurosciences and Experimental Therapeutics, Institut d' Investigacions Biomèdiques de Barcelona, Consejo Superior de Investigaciones Científicas, Barcelona 08036, Spain

[9]Instituto de Investigación Sanitaria del Hospital Clínico San Carlos (IdISSC), Madrid 28040, Spain

[10]Department of Biomedicine, School of Medicine, Institute of Neuroscience, University of Barcelona, Barcelona 08036, Spain

[11]Centre for Endocrinology, William Harvey Research Institute, Barts and The London School of Medicine and Dentistry, Queen Mary University of London, EC1M 6BQ London, United Kingdom

[12]Institut National de la Santé et de la Recherche Médicale (INSERM) and University of Bordeaux, NeuroCentre Magendie, Physiopathologie de la Plasticité Neuronale, U1215, Bordeaux 33077, France

Correspondence: Manuel Guzmán (mguzman@quim.ucm.es), Ignacio Rodríguez-Crespo (jirodrig@quim.ucm.es)

Number of pages: 55

Number of figures, tables, multimedia, and 3D models: 10 figures, 2 tables, 0 multimedia, 0 3D models

Number of words for abstract, introduction, and discussion: 209 abstract, 583 introduction, 682 discussion

Conflict of interest statement

The authors declare no competing financial interests.

Acknowledgments

This work was supported by the Spanish *Ministerio de Ciencia e Innovación* (MICINN/FEDER; grants RTI2018-095311-B-I00 to MG, SAF-2017-87629-R to EIC and VC, PID2019-106404RB-I00 to LU, BFU 2017-83292-R to JS-P, and RTI2018-094374-B-I00 to SG), *Centro de Investigación Biomédica en Red sobre Enfermedades Neurodegenerativas* (CIBERNED/ISCIII; grant PI2018/01 to MG, SG, and GMe), and UK Research and Innovation Biotechnology and Biological Sciences Research Council (grant BB/R006946/1 to PJM). LB and GM were supported by INSERM. CC-I and IBM were supported by contracts from the Spanish *Ministerio de Universidades* (*Formación de Profesorado Universitario* Program, references FPU16/02593 and FPU15/01833, respectively). RB-G was supported by a contract from the Spanish *Ministerio de Ciencia e Innovación* (MICINN/FEDER; *Juan de la Cierva* Program). We are indebted to Lucía Rivera, Elena García-Taboada, Carlos Montero, Andrea Macías, Alicia Álvaro, Guillermo Martín-Migallón, and Susana Muñoz-Morales for expert laboratory assistance.

Abstract

Cannabinoids, the bioactive constituents of cannabis, exert a wide array of effects on the brain by engaging type-1 cannabinoid receptor (CB_1R). Accruing evidence supports that cannabinoid action relies on context-dependent factors such as the biological characteristics of the target cell, suggesting that cell population-intrinsic molecular cues modulate CB_1R-dependent signaling. Here, by using a yeast two-hybrid-based high-throughput screening, we identified BiP as a potential CB_1R-interacting protein. We next found that CB_1R and BiP interact specifically *in vitro*, and mapped the interaction site within the CB_1R *C*-terminal (intracellular) domain and the BiP *C*-terminal (substrate-binding) domain-α. BiP selectively shaped agonist-evoked CB_1R signaling by blocking an "alternative" $G_{q/11}$ protein-dependent signaling module, while leaving the "classical" $G_{i/o}$ protein-dependent inhibition of the cAMP pathway unaffected. *In situ* proximity ligation assays conducted on brain samples from various genetic mouse models of conditional loss or gain of CB_1R expression allowed to map CB_1R-BiP complexes selectively on terminals of GABAergic neurons. Behavioral studies using cannabinoid-treated $BiP^{+/-}$ mice supported that CB1R-BiP complexes modulate cannabinoid-evoked anxiety, one of the most frequent undesired effects of cannabis. Altogether, by identifying BiP as a CB1R-interacting protein that controls receptor function in a signaling pathway- and neuron population-selective manner, our findings may help to understand the striking context-dependent actions of cannabis in the brain.

Significance Statement

Cannabis use is increasing worldwide, so innovative studies aimed to understand its complex mechanism of neurobiological action are warranted. Here, we found that cannabinoid CB_1 receptor (CB_1R), the primary molecular target of the bioactive constituents of cannabis, interacts specifically with an intracellular protein called BiP. The interaction between CB_1R and BiP occurs selectively on terminals of GABAergic (inhibitory) neurons, and induces a remarkable shift in the CB_1R-associated signaling profile. Behavioral studies conducted in mice support that CB_1R-BiP complexes act as fine-tuners of anxiety, one of the most frequent undesired effects of cannabis use. Our findings open a new conceptual framework to understand the striking context-dependent pharmacological actions of cannabis in the brain.

Introduction

Preparations of the hemp plant *Cannabis sativa* L. have been used by humankind for millennia. During the last decades there has been a strong renaissance in the study of the molecular and pharmacological bases of cannabinoid action, and, in concert, many countries have approved the use of cannabinoid-based medicines and standardized preparations of medicinal cannabis (Hill, 2015; Abrams, 2018). Both the therapeutic and the adverse effects of cannabis are mostly attributed to a single molecule, Δ^9-tetrahydrocannabinol (THC) (Mechoulam et al., 2014). This compound engages and activates two specific G protein-coupled receptors (GPCRs), designated as cannabinoid CB_1 receptor (CB1R) and cannabinoid CB_2 receptor (CB2R) (Pertwee et al., 2010). CB1R is one of the most abundant GPCRs in the mammalian brain (Katona and Freund, 2008; Pertwee et al., 2010; Dudok et al., 2015). It mediates a large number of pharmacological effects of THC, and, upon binding endocannabinoids (anandamide and 2-arachidonoylglycerol), participates in the physiological control of multiple processes such as motor behavior, learning and memory, fear and anxiety, pain, food intake, and energy metabolism (Piomelli, 2003; Mechoulam et al., 2014).

The precise molecular mechanism of CB1R action remains unsolved. For example, CB1R couples to the inhibitory family of heterotrimeric G proteins ($G_{i/o}$), but its expression and signaling efficacy differs remarkably between excitatory and inhibitory neurons (Steindel et al., 2013), which could explain, at least in part, the widely reported biphasic effects elicited by THC and other CB1R agonists (Bellocchio et al., 2010; Rey et al., 2012; Mechoulam and Parker, 2013). Likewise, under different cellular settings, CB1R can signal through other G protein families as $G_{q/11}$ and G_s (Lauckner et al., 2005; Priestley et al., 2017). Furthermore, CB1R activation protects neurons from death in a wide array of pathological conditions (Fernández-Ruiz, 2019), while it triggers apoptosis

of brain cancer cells (Velasco et al., 2012). How these striking differences in signaling efficacy, G-protein coupling, and biological response occur is not understood. Altogether, these observations suggest a cell population-selective action of CB1R colligated to the physiopathological context of the target cell expressing the receptor. Understanding how CB1R evokes such varying responses is important to clarify the neurobiological role of the endocannabinoid system and, potentially, to improve the design of CB1R-targeted therapies.

Interaction with regulatory proteins represents one of the pivotal molecular processes by which GPCR-evoked signaling is affected. Diverse subsets of these interacting proteins assist GPCRs during biosynthesis, trafficking, activation, desensitization, and degradation (Maurice et al., 2011). Aside from the most ubiquitous GPCR-associated proteins (*i.e.*, G proteins, β-arrestins, and GPCR kinases), specific interacting partners have been identified for particular types of receptors (*e.g.*, NHERF proteins for adrenergic receptors and others, and Homer proteins for metabotropic glutamate receptors and others) (Wheeler et al., 2007; Magalhaes et al., 2012) . Regarding CB1R, several intracellular proteins (led by CRIP1a) (Howlett et al., 2010; Guggenhuber et al., 2016), as well as membrane-anchored GPCRs (*e.g.*, serotonin 5-HT_{2A} and adenosine A_{2A} receptors) (Viñals et al., 2015; Moreno et al., 2018), have been proposed as receptor interactors. However, most studies on these putative protein complexes have been conducted *in vitro*, and only subtle effects have been unraveled so far *in vivo*.

Here, we hypothesized that unidentified neuron population-specific CB1R-interacting proteins modulate cannabinoid signaling in the brain. By using a yeast two-hybrid (Y2H)-based approach, complemented with a wide array of molecular, genetic, pharmacological, and behavioral procedures, we identified the protein BiP as a new

modulator of biased signaling of CB1R, and defined the molecular features, signal-transduction consequences, neuroanatomical mapping, and behavioral outcomes of the CB1R-BiP interaction.

Materials and Methods

Gene constructs

Y2H vectors were generated by PCR and subsequent restriction cloning by using pGBT9 and pGAD as vectors (ClonTech, TaKaraBio, Mountain View, CA, USA). Short amino-acid stretches (CB1R mutants) were ligated by using long annealing oligonucleotides with protruding overhangs. The cDNA encoding full-length BiP was provided by Dr. Valerie Petegnief (Institute for Biomedical Research of Barcelona, Barcelona, Spain), and expression vectors encoding non-tagged (pcDNA3.1+ backbone; Thermo Fisher Scientific, Waltham, MA, USA), GFP-tagged (pEGFP-C2 backbone; ClonTech) and recombinant bacterial-expression [pBH4 backbone (Merino-Gracia et al., 2016b)] versions were built as well by PCR and restriction cloning. BiP-ΔIR comprised BiP amino acids 1-308. 3XFLAG-tagged versions were obtained by using IVA cloning (García-Nafría et al., 2016) with pcDNA3.1+ plasmids as templates. pcDNA3.1-HA-CB1R, pcDNA3.1-CB1R-myc, CB1R-Rluc, CB1R-GFP and pcDNA3.1-A1R constructs had been generated previously in our laboratory. Single phosphomimetic mutants of CB1R-CTD, as well as the CB1R-S452D-Rluc construct, were obtained through Quickchange mutagenesis with the aforementioned plasmids as templates. pcDNA3.1-CB2R was provided by Dr. Cristina Sánchez (Complutense University of Madrid, Madrid, Spain) and used to construct the corresponding Y2H vector. pCEFL-GFP and pCEFL-GFP-GRK2 plasmids were given by Dr. J. Silvio Gutkind (University of California San Diego, CA, USA). All constructs were validated by Sanger sequencing before use.

Yeast two-hybrid (Y2H)

Screening of the library was performed following the manufacturer's instructions (MatchMaker system, TaKaraBio, Mountain View, CA, USA). Plasmids of positive transformants were isolated and subsequently sequenced by standard procedures. Directed Y2H experiments were conducted as previously reported (Merino-Gracia et al., 2016a). Yeasts were transformed with plasmids containing the GAL4 binding domain and the GAL4 activation domain following a lithium acetate-based method. Double transformants were placed on Leu/Trp/His-deficient plates in the presence of 12 mM 3-aminotriazole (triple dropout plates) as well as only Leu/Trp-deficient plates. Interacting proteins expressed within the same yeast allowed colonies that could rescue growth in triple-dropout plates and were capable to hydrolyse X-Gal.

Protein expression and purification

pBH4 plasmids encoding His6-tagged BiP, BiP-IR (amino acids 497-654) or CB1R-CTD (amino acids 400-472) were used to transform competent BL21 DE3 *Escherichia coli*. Typically, 2 liters of bacterial culture in 2xYT (16 g/L tryptone, 10 g/L yeast extract, 5 g/L NaCl, pH 7.0) were used for recombinant protein expression. Protein expression was induced by addition of 0.5 mM isopropyl 1-thio-β-D-galactopyranoside (Panreac Química S.A.U., Barcelona, Spain) and incubation overnight at 30 °C with 250 rpm aeration rate. Bacterial cells were pelleted and frozen at −20 °C until used for protein purification.

Bacterial cell lysis was conducted in ice-cold lysis buffer (100 mM Tris-HCl, 100 mM NaCl, 10 mM imidazole, pH 7.0) with continuous shaking in the presence of protease inhibitors (1 µg/mL aprotinin, 1 µg/mL leupeptin, 200 µM PMSF), 0.2 g/l lysozyme and 5 mM β-mercaptoethanol, followed by 4 cycles of sonication on ice. The cell lysate was clarified by centrifugation at 10,000*g* and filtration through porous paper.

Recombinant His6-tagged proteins were sequentially purified on a nickel-nitrilotriacetic acid affinity column. After extensive washing (50 mM Tris, 100 mM NaCl, 25 mM imidazole, pH 7.0), proteins were eluted with elution buffer (50 mM Tris, 100 mM NaCl, 250 mM imidazole, pH 7.0; supplemented with protease inhibitors). Protein purity was confirmed by SDS-PAGE and Coomassie Brilliant Blue or Silver staining. Pure protein solutions were concentrated by centrifugation in Centricon® tubes (Millipore, Burlington, MA, USA).

Fluorescence polarization

His6-tagged CB1R-CTD (amino acids 400-472) was labelled with 5-(Iodoacetamido)fluorescein (5-IAF) by standard procedures. Briefly, the FITC dye was dissolved in DMSO and the labelling reaction was performed in sodium bicarbonate buffer, pH 9.0, with a 3-fold molar excess of dye for 1 hour at 25 °C, protected from light. Subsequently, a 1.00-Da cut-off dialysis membrane was used to eliminate non-reacted 5-IAF compound. After extensive dialysis, the concentration of the labeled peptide was calculated using the value 68,000 $cm^{-1}M^{-1}$ as the molar extinction coefficient of the dye at pH 8.0 at 494 nm. Saturation binding experiments were performed essentially as described (Merino-Gracia et al., 2016a) with a constant concentration of 100 nM 5-IAF-CB1R-CTD. The fluorescence polarization values obtained were fitted to the equation $(FP\text{-}FP_0) = (FP_{Max}\text{-}FP_0)[BiP \text{ or } BiP\text{-}IR]/(K_d + [BiP \text{ or } BiP\text{-}IR])$, where FP is the measured fluorescence polarization, FP_{Max} is the maximal fluorescence polarization value, FP_0 is the fluorescence polarization in the absence of added BiP or BiP-IR, and K_d is the dissociation constant as determined with GraphPad Prism v8.0.1 (GraphPad Software, San Diego, CA, USA). FP was expressed as milli-FP units (mFP; net FP x 1,000). Each representative curve shown is the mean of three internal replicates.

Cell culture, transfection, and incubation

The HEK-293T cell line was obtained from the American Type Culture Collection (Manassas, VA, USA). Cells were grown in DMEM supplemented with 10% FBS (Thermo Fisher Scientific), 1% penicillin/streptomycin, 1 mM Na-pyruvate, 1 mM L-glutamine, and essential medium non-essential amino acids solution (diluted 1/100) (all from Invitrogen, Carlsbad, CA, USA). Cells were maintained at 37ºC in an atmosphere with 5% CO_2 in the presence of the selection antibiotic (zeocin at 0.22 mg/mL, Thermo Fisher Scientific), and were periodically checked for the absence of mycoplasma contamination. Cell transfections were conducted with polyethyleneimine (Polysciences inc. Warrington, PA, USA) in a 4:1 mass ratio to DNA according to the manufacturer's instructions. Double transfections were performed with equal amounts of the two plasmids. In all cases, 48 hours after transfection, cells were washed twice in quick succession, detached, and harvested for further procedures. To control cell number, protein concentration in the samples was determined with a Bradford assay kit (Bio-Rad, Hercules, CA, USA).

Drug treatments to assess CB1R-evoked signaling were conducted as follows. A 10 cm-diameter plate of transfected cells was trypsinized and seeded on a 6-well plate at a density of $0.75x10^6$ cells per well. Six hours later, cells were serum-starved overnight. Then, WIN-55,212-2 (Tocris Bioscience, Bristol, UK; 100 nM final concentration) or vehicle (DMSO, 0.1% v/v final concentration) was added for 5, 10 or 15 minutes. $G\alpha_{q/11}$ inhibition was achieved by adding YM-254890 (Focus Biomolecules, LLC, Plymouth Meeting, PA, USA; 1 µM final concentration) or vehicle (DMSO, 0.1% v/v final concentration) 30 minutes before WIN-55,212-2 (100 nM final concentration) or vehicle (DMSO, 0.1% v/v final concentration). All incubations were carried out in

252 triplicate. Cells were subsequently washed with ice-cold PBS, snap-frozen in liquid
253 nitrogen, and harvested at -80 °C for Western blot analyses.
254
255 ***In situ proximity ligation assay (PLA)***
256 BiP-CB1R complexes were detected by using the Duolink In Situ PLA Detection Kit
257 (Sigma-Aldrich, St. Louis, MO, USA) following the manufacturer's instructions.
258 Synaptosomal preparations were incubated with a rabbit-anti-CB1R antibody (1:500,
259 Frontier-Institute, Ishikari, Hokkaido, Japan #CB1-Rb-Af530) and a mouse anti-
260 GRP78/BiP antibody (1:500, Santa Cruz Biotechnology; Dallas, TX, USA #sc-376768).
261 Negative controls were performed with just one primary antibody. Ligations and
262 amplifications were performed with In Situ Detection Reagent Red (Sigma-Aldrich), and
263 coverslips were mounted in DAPI-containing mounting medium. Samples were analyzed
264 with a Leica SP2/SP8 confocal microscope (Leica Microsystems, Mannheim, Germany).
265 For each field of view a stack of two channels (one per staining) and 9 to 13 *Z*-stacks
266 with a step size of 0.3 µm were acquired with an 63x oil-immersion objective and
267 processed with ImageJ software (National Institutes of Health, Bethesda, MD).
268 Representative images for each condition were prepared for figure presentation by
269 applying color adjustments uniformly with Adobe Photoshop vCS6 (Berkeley, CA, USA).
270 For PLA imaging in brain sections, mice were deeply anesthetized and
271 immediately perfused transcardially with PBS followed by 4%
272 paraformaldehyde/phosphate buffer. Brains were removed and post-fixed overnight in
273 the same solution, cryoprotected by immersion in 10, 20, 30% gradient sucrose (24
274 hours for each sucrose gradient) at 4 °C, and then frozen in dry ice-cooled
275 methylbutane. Serial coronal or sagittal cryostat sections (30 µm-thick) through the
276 whole brain were collected in cryoprotective solution and stored at -20°C until PLA

experiments were performed. Immediately before the assay, mouse brain sections were mounted on glass slides, washed in PBS, permeabilized with PBS containing 0.01% Triton X-100 for 10 minutes, and successively washed with PBS. Interactions were detected with Duolink In Situ PLA Detection and In Situ Detection Reagent Red Kits. A mixture of the primary antibodies [mouse anti-GRP78/BiP antibody (1:100, Santa Cruz Biotechnology #sc-376768) and rabbit anti-CB1R antibody (1:100, Thermo Scientific, Fremont, CA, USA #PA1-745)] was used. Samples were analyzed in a Leica SP2 confocal microscope (Leica Microsystems) equipped with an apochromatic 63x oil-immersion objective (1.4 numerical aperture), and a 405 nm and a 561 nm laser lines. For each field of view a stack of two channels (one per staining) and 9 to 13 *Z*-stacks with a step size of 1 µm were acquired. Images were opened and processed with Image J software (NIH). Quantification of cells containing one or more red dots versus total cells (blue nuclei) was determined by using the Fiji package (http://pacific.mpi-cbg.de). Nuclei and red dots were counted on the maximum projections of each image stack. After getting the projection, each channel was processed individually. The blue nuclei and red dots were segmented by filtering with a median filter, subtracting the background, enhancing the contrast with the Contrast Limited Adaptive Histogram Equalization (CLAHE) plug-in, and finally applying a threshold to obtain the binary image and the regions of interest.

Bioluminescence Resonance Energy Transfer (BRET)

HEK-293T cells growing in 6-well plates were transiently cotransfected with a constant amount of cDNA encoding the receptor fused to Rluc protein and with increasingly amounts of GFP-BiP-IR. To quantify protein-GFP expression, cells (20 µg total protein) were distributed in 96-well microplates (black plates with a transparent bottom) and the

fluorescence was read in a Fluostar Optima fluorimeter (BMG Labtech, Offenburg, Germany) equipped with a high-energy xenon flash lamp using a 10-nm bandwidth excitation filter at 410 nm for protein-GFP reading. Protein-fluorescence expression was determined as fluorescence of the sample minus the fluorescence of cells expressing only the BRET donor. For BRET measurements, cells (20 µg of protein) were distributed in 96-well microplates (Corning 3600, White plates; Sigma) and BRET signal was collected 1 minute after addition of 5 µM DeepBlueC (Molecular Probes, Eugene, OR) using a Mithras LB 940 reader (Berthold Technologies, Bad Wildbad, Germany), that allows the integration of the signals detected in the short-wavelength filter at 400 nm and the long-wavelength filter at 510 nm. To quantify receptor-Rluc expression luminescence readings were also performed after 10 minutes of adding 5 µM DeepBlueC (Molecular Probes, Eugene, OR). The net BRET is defined as [(long-wavelength emission)/(short-wavelength emission)]-Cf where Cf corresponds to [(long-wavelength emission)/(short-wavelength emission)] for the Rluc construct expressed alone in the same experiment. BRET is expressed as milli BRET units (mBU; net BRET x 1,000). In BRET curves BRET was expressed as a function of the ratio between fluorescence and luminescence (GFP/Rluc). To calculate maximal BRET from saturation curves, data was fitted using a non-linear regression equation and assuming a single phase with GraphPad Prism software v8.0.1. Each representative curve shown is the mean of three internal replicates.

Western blot and co-immunoprecipitation

Samples for Western blotting were prepared on ice-cold lysis buffer (50 mM Tris-HCl, 1 mM EDTA, 1 mM EGTA, 0.1% Triton X-100, 50 mM NaF, 10 mM Na-glycerophosphate, 5 mM Na-pyrophosphate, 1 mM Na-orthovanadate, pH 7.5). Cell lysates were clarified

by centrifugation at 12,000*g* for 15 minutes (4 °C) and total protein was quantified using the Bradford assay. Then, 5 to 20-µg aliquots of total protein, boiled for 5 minutes at 95 °C and prepared in 5x Laemmli Sample Buffer, were resolved by using SDS-PAGE and transferred to PVDF membranes. Membranes were blocked with 5% defatted milk (w/v) or 5% BSA (w/v) in TBS-Tween-20 (0.1%) for 1 hour and incubated overnight with the following antibodies and dilutions: anti-phospho-ERK1/2 (1:1,000, CST*,* Danvers, MA, USA #9101), anti-ERK1/2 (1:1,000, CST #4696), anti-phospho-p70S6K (1:1,000, CST#9206), anti-phospho-CREB (1:1,000, CST #9198), anti-BiP (1:1,000, Sigma-Aldrich #G8918), anti-GFP (1:1000, Thermo Scientific #MA5-15256), anti-α-tubulin (1:10,000, Sigma-Aldrich #T9026), anti-β-actin (1:10,000, Sigma-Aldrich #A5441), anti-FLAG M2 (1:1,000, Sigma-Aldrich #F3165), anti-HA (1:1,000, CST #3724S), and anti-calnexin (1:1,000, Santa Cruz Biotechnology #SC-6465). All antibodies were prepared in TBS-Tween-20 (0.1%) with 5% BSA (w/v). Membranes were then washed three times with TBS-Tween-20 (0.1%), and HRP-labeled secondary antibodies, selected according to the species of origin of the primary antibodies (Sigma-Aldrich #NA-931-1 and #NA-934V), were added for 1 hour at a 1:5,000 dilution in TBS-Tween-20 (0.1%) at room temperature. Finally, protein bands were detected by incubation with an enhanced chemiluminescence reagent (Bio-Rad) and densitometric analysis of the relative expression of the protein of interest *vs.* the corresponding loading control was performed with ImageJ software. Western blot images were cropped for clarity. Electrophoretic migration of molecular weight markers is depicted on the left-hand side of each blot.

For co-immunoprecipitation experiments, 48 hours after transfection, cells were lysed on ice-cold GST buffer (50 mM Tris-HCl, 10% glycerol v/v, 100 mM NaCl, 2 mM $MgCl_2$, 1% v/v NP-40, pH 7.4), supplemented with protease inhibitors. Cell lysates were clarified by centrifugation at 12,000*g* for 15 minutes (4 °C) and total protein was

quantified with Bradford assay. Twenty-µg aliquots were collected to check for transfection levels (whole-cell lysates), and 1 mg of total protein was incubated with 20 µL of HA-agarose beads (Thermo Scientific #26181) or FLAG M2 agarose beads (Sigma-Aldrich #A2220) for 2-4 hours at 4 °C with a final protein concentration of 1 mg/mL. Beads were subsequently washed 3 times with lysis buffer and eluted with 30 µL of 2x Laemmli Sample Buffer without β-mercaptoethanol and 5 minutes of sample boiling. Ten µL of the elution was further analyzed by Western blotting as previously described. GFP immunoprecipitation was performed analogously, with a pre-clarification step on 30 µL of Protein A/G (GE Healthcare, Chicago, IL, USA #17061801), followed by overnight incubation of the remaining supernatant with 1 µg of anti-GFP antibody (produced in-home), and 2-4 hours of incubation with 30 µL of Protein A/G mixture. The rest of the steps were identical to those mentioned above.

Dynamic mass redistribution (DMR)

The cell-signaling signature was determined using an EnSpire® Multimode Plate Reader (PerkinElmer, Waltham, MA, USA) by a label-free technology. Cellular mass movements induced upon receptor activation were detected by illuminating the underside of the biosensor with polychromatic light and measured as changes in wavelength of the reflected monochromatic light that is a sensitive function of the index of refraction. The magnitude of this wavelength shift (herein measured in picometers) is directly proportional to the amount of DMR. Briefly, 24 hours before the assay, cells were seeded at a density of 10,000 cells per well in 384-well sensor microplates with 30 µL growth medium and cultured for 24 h (37°C, 5% CO_2) to obtain 70-80% confluent monolayers. Previous to the assay, cells were washed twice with assay buffer (HBSS with 20 mM Hepes, pH 7.15) and incubated for 2 h in 30 µL per well of assay-buffer with

0.1% DMSO in the reader at 24 °C. Hereafter, the sensor plate was scanned, and a baseline optical signature was recorded before adding 10 µL of the test compound dissolved in assay buffer containing 0.1% DMSO. Then, DMR responses were monitored along time, and kinetic data were analysed using EnSpire Workstation Software v4.10. Each representative curve shown is the mean of three internal replicates.

Phosphoprotein array

Cells transfected with CB1R-GFP and BiP-IR (or control) plasmids were treated with WIN-55,212-2 (100 nM final concentration) or vehicle (DMSO, 0.1% v/v final concentration) as described above for 5 and 15 minutes. Samples from two independent experiments were processed separately by using 350 µg of total protein per experimental condition, following the instructions of the Proteome Profiler Human Phospho-Kinase Array Kit (R&D, Bio-techne, Minneapolis, MN, USA #ARY003C). Densitometric analysis of the relative phosphorylation levels *vs.* the corresponding housekeeping controls and between WIN-55,212-2/vehicle treatments was performed with ImageJ software and the Protein Array Analyzer toolset.

Cellular and subcellular fraction preparations

Membrane preparations for G protein-coupling assays were obtained from HEK-293T-cell pellets or adult mouse-hippocampus tissue specimens. Frozen samples were thawed at 4 °C and homogenized with a glass/teflon grinder (IKA labortechnik, Satufen, Germany), 10 strokes at maximum speed, in 30 volumes of homogenization buffer (250 mM sucrose, 50 mM Tris-HCl, 1 mM EGTA, 3 mM $MgCl_2$, 1 mM DTT, pH 7.4). The homogenates were centrifuged at 1,100*g* for 10 minutes at 4 °C. The pellets were

discarded, and the supernatants were re-centrifuged at 40,000*g* for 10 minutes at 4 °C. The resultant pellets were resuspended in 20 volumes of ice-cold centrifugation buffer (50 mM Tris-HCl, 1 mM EGTA, 3 mM $MgCl_2$, 1 mM DTT, pH 7.4) with a glass stick and recentrifuged at 40,000*g* for 10 minutes at 4 °C. The pellets obtained were then resuspended in 5 volumes of centrifugation buffer. Protein content was determined by the Bradford method. Finally, aliquots of 0.5, 1.0 and 2.0 mg protein were centrifuged at 21,000*g* for 15 minutes at 4 °C. The supernatant layer was carefully discarded, and the pellets were stored at -80 °C until assayed.

Total, cytosolic and ER fractions from hippocampus, cortex and striatum of the adult mouse brain were obtained by lysing the corresponding regions through sonication in 2 mL of ice-cold MTE buffer (270 mM D-mannitol, 10 mM Tris-HCl, 0.1 mM EDTA, pH 7.4). Tissue extracts were centrifuged (1,400*g*, 10 minutes, 4 °C), and the supernatant (total cell lysate) was re-centrifuged (15,000*g*, 10 minutes, 4 °C) to separate the pelleted mitochondrial crude fraction. Isolation of ER from cytosol was achieved by loading the sample in a sucrose gradient (2 M – 1.5 M – 1.3 M) and conducting an ultracentrifugation step (152,000*g*, 70 minutes, 4 °C). The ER fraction appears as a band at the 1.5 M/1.3 M sucrose interphase, while the cytosolic fraction remains at the top of the tube. Both fractions were collected, in the case of the ER with the aid of a syringe with a 20G needle, and the ER fraction was further purified by an additional ultracentrifugation step (126,000*g*, 45 minutes, 4 °C). The ER-containing pellet was resuspended in 100 µL of PBS and immediately frozen. Likewise, aliquots of total cell lysate and cytosolic fractions were collected throughout the process and immediately frozen. Samples were kept at -80 ºC for Western blot analysis.

Striatal, hippocampal and cortical synaptosomes were isolated from adult CB1R-KO mice and CB1R-WT control littermates, plated on poly-L-lysine-covered coverslips,

fixed in 4% paraformaldehyde and characterized as described (Martín et al., 2010). PLA assays were conducted as described above.

Antibody-capture [^{35}S]GTPγS scintillation proximity assay

Specific activation of different subtypes of Gα protein subunits ($G\alpha_{i1}$, $G\alpha_{i2}$, $G\alpha_{i3}$, $G\alpha_{o}$, $G\alpha_{q/11}$, $G\alpha_{s}$, $G\alpha_{z}$, and $G\alpha_{12/13}$) was determined by using a homogeneous protocol of [^{35}S]GTPγS scintillation proximity assay coupled to the use of the following antibodies: mouse monoclonal anti-$G\alpha_{i1}$ (1:20, Santa Cruz Biotechnology #sc-56536), rabbit polyclonal anti-$G\alpha_{i2}$ (1:20; Santa Cruz Biotechnology #sc-7276), rabbit polyclonal anti-Gαi3 (1:30, Antibodies on-line #ABIN6258933), mouse monoclonal anti-$G\alpha_{o}$ (1:40, Santa Cruz Biotechnology #sc-393874), mouse monoclonal anti-$G\alpha_{q/11}$ (1:20, Santa Cruz Biotechnology #sc-515689), rabbit polyclonal anti-$G\alpha_{s}$ (1:20, Santa Cruz Biotechnology #sc-383), rabbit polyclonal anti-$G\alpha_{z}$ (1:20, Santa Cruz Biotechnology #sc-388), and rabbit polyclonal anti-$G\alpha_{12/13}$ (1:20 Santa Cruz Biotechnology sc-28588). [^{35}S]GTPγS binding was measured in 96-well isoplates (PerkinElmer Life Sciences, Maanstraat, Germany) and a final volume of 200 µL containing 1 mM EGTA, 3 mM $MgCl_2$, 100 mM NaCl, 0.2 mM DTT, 50 mM Tris–HCl, pH 7.4, 0.4 nM [^{35}S]GTPγS, 10 µg of protein per well, and different concentrations of GDP (between 50 and 100 µM) depending on the Gα subunit subtype tested. At the end of the 2-hour incubation period (at 30 °C), 20 µL of 1% Igepal plus 0.1% SDS was added to each well, and plates were incubated at 22 °C for 30 minutes with gentle agitation. The specific antibody for the Gα subunit of interest was then added to each well before an additional 90-minute incubation period at room temperature. Polyvinyltoluene (PVT) SPA beads coated with protein A (PerkinElmer, S.L., Tres Cantos, Madrid, Spain) were then added (0.75 mg of beads per well), and plates were incubated for 3 hours at room temperature with gentle agitation.

Finally, plates were centrifuged (5 minutes at 1,000*g*), and the bound radioactivity was detected on a MicroBeta TriLux scintillation counter (PerkinElmer S.L., Tres Cantos, Madrid, Spain). To determine their effect on [^{35}S]GTPγS binding to the different Gα subunit subtypes in the different experimental conditions, a single submaximal concentration (10 μM) of WIN-55,212-2 was used, either alone or in the presence of the CB1R antagonist O-2050 (10 μM) as control. Nonspecific binding was defined as the remaining [^{35}S]GTPγS binding in the presence of 10 μM unlabelled GTPγS. For each Gα protein, specific [^{35}S]GTPγS binding values were transformed to percentages of basal [^{35}S]GTPγS binding values (those obtained in the presence of vehicle).

Determination of cAMP concentration

Homogeneous time-resolved fluorescence energy transfer (HTRF) assays were performed using the Lance Ultra cAMP kit (PerkinElmer). HEK-293T cells (1,000 per well), growing in medium containing 50 μM zardeverine, were incubated in triplicate for 15 minutes in white ProxiPlate 384-well microplates (PerkinElmer) at 25°C with vehicle or WIN-55,212-2 (100 nM final concentration) before adding vehicle or forskolin (0.5 μM final concentration) and incubating for 15 additional minutes. Fluorescence at 665 nm was analyzed on a PHERAstar Flagship microplate reader equipped with an HTRF optical module (BMG Lab technologies, Offenburg, Germany).

Animals

All the experimental procedures used were performed in accordance with the guidelines and with the approval of the Animal Welfare Committees of Universidad Complutense de Madrid and Comunidad de Madrid, as well as of Universitat de Barcelona and Generalitat de Catalunya, and in accordance with the directives of the Spanish

Government and the European Commission. BiP$^{+/-}$ (herein referred to as BiP-HET) mice were purchased from The Jackson Laboratory (Bar Harbor, ME, USA #019549). We also used CB1R$^{floxed/floxed}$ (herein referred to as CB1R-floxed) mice, CB1R$^{floxed/floxed;CMV\text{-}Cre}$ (herein referred to as CB1R-KO) mice, conditional CB1R$^{floxed/floxed;Nex1\text{-}Cre}$ (herein referred to as Glu-CB1R-KO) mice, and conditional CB1R$^{floxed/floxed;Dlx5/6\text{-}Cre}$ (herein referred to as GABA-CB1R-KO) mice (Monory et al., 2006); as well as Stop-CB1R, Stop-CB1R$^{EIIa\text{-}Cre}$ (herein referred to as CB1R-RS) mice, conditional Stop-CB1R$^{Nex1\text{-}Cre}$ (herein referred to as Glu-CB1R-RS) mice, and conditional Stop-CB1R$^{Dlx5/6\text{-}Cre}$ (herein referred to as GABA-CB1R-RS) mice, to allow CB1R gene-expression rescue from a CB1R-null background (Ruehle et al., 2013; De Salas-Quiroga et al., 2015). Animal housing, handling and assignment to the different experimental groups were conducted as described (Ruiz-Calvo et al., 2018). Adequate measures were taken to minimize pain and discomfort of the animals.

In situ hybridization histochemistry

For *in situ* hybridization histochemistry (ISHH), 14 µm-thick coronal whole-brain tissue sections were obtained from adult C57BL/6 mice (Janvier Laboratories, France), cut on a microtome-cryostat (Microm HM500 OM, Walldorf, Germany), thaw-mounted on 3-aminopropyltriethoxysilane (APTS)-coated slides (Sigma-Aldrich), and kept at -20 °C until further processing. The oligonucleotides complementary to the mRNAs encoding BiP, CB1R, and GABAergic or glutamatergic markers are listed in Table 1. Oligonucleotides for each mRNA were labeled at their 3´-end by using [α-^{33}P]dATP (3000 Ci/mmol, Hartmann Analytic GmbH, Braunschweig, Germany). Labeled probes were purified on ProbeQuant G-50 Micro Columns (GE Healthcare, Buckinghamshire, UK). ISHH procedures were performed as described (Sanabra and Mengod, 2011). For

autoradiography, hybridized sections were exposed to Biomax-MR (Kodak, Rochester, NY, USA) films for 1-10 days at -70 °C with intensifying screens. Double *in situ*-hybridized sections were processed as described (Reyes-Irisarri et al., 2007). They were exposed in the dark for 4-6 weeks at 4°C. Images from autoradiograms were obtained by using a Wild 420 macroscope (Leica Microsystems, Wetzlar, Germany) equipped with a digital camera (DXM1200 F, Nikon, Tokyo, Japan) and ACT-1 Nikon software. Microphotography was performed with an Olympus BX51 Stereologic Microscope (Olympus, Tokyo, Japan) equipped with a digital camera (DP71, Olympus) or with a Zeiss Axioplan microscope (Germany) equipped with an Olympus XC50 digital camera. Figures were assembled using Adobe Photoshop (Adobe Systems, San Jose, CA, USA). Only contrast and brightness were uniformly adjusted in order to optimize images.

Behavioral tests

Adult male mice (3-4 month-old) were injected i.p. with vehicle (1% v/v DMSO in 1:18 v/v Tween-80/saline solution) or 10 mg/kg THC (THC Pharm). The “cannabinoid tetrad” was assessed, starting 30 minutes after injection, following standard guidelines (Metna-Laurent et al., 2017). First, the open-field test was conducted for 10 minutes in an arena of 70 x 70 cm. To evaluate anxiety-like behaviors, the number of entries of the animal into the central part of the arena (25 x 25 cm) relative to total ambulation was assessed, one entry being counted when the animal had placed at least both forelimbs in the square. Next, analgesia was assessed as the latency to paw licking in the hot-plate paradigm at a constant temperature of 52 °C. Then, for the catalepsy test, the animal was placed with both forelimbs leaning on a bar situated at a height of 3.5 cm. Immobility was considered maximal when the animal exceeded 60 seconds of immobility, and null when the immobility time was lower than 5 seconds. In all cases, 3 attempts were

performed, and the maximal immobility time was selected as the representative value. Finally, body temperature was measured with a rectal thermometer and compared to the basal, pre-injection value.

The elevated plus maze test was evaluated 4 hours after acute i.p. injection of vehicle or THC (10 mg/kg). The maze consisted of a cross-shaped plastic device with two opposite open arms (30-cm long, 5-cm wide) and two opposite closed arms (30 cm-long, 5-cm wide, 16-cm tall walls), connected by a central structure (5 x 5 cm), and elevated 50 cm from the floor. Each mouse was placed in the center of the maze, facing one of the open arms, and the exploratory behavior of the animal was video-recorded for 5 minutes. The number and duration of entries was measured separately for the open arms and the closed arms. One arm entry was registered when the animal had placed both forepaws in the arm.

In all cases, animals were assigned randomly to the different treatment groups, and all experiments were performed in a blinded manner for genotype and pharmacological treatment. All tests were video-recorded for subsequent blinded analysis using Smart3.0 v3.00.6 Software (Panlab, Barcelona, Spain).

Experimental design and statistical analyses

Unless otherwise specified, data are presented as mean ± SEM. Statistical comparisons were conducted by one-way or two-way ANOVA with Tukey's *post hoc* test, or by Student's *t* test, as indicated in each case. All datasets were tested for normality (Kolmogorov-Smirnov's test) and homoscedasticity (Levene's test) prior to analysis. For clarity, only *p* values lower than 0.05 were considered statistically significant. The sample size for each experiment was estimated on the basis of previous studies conducted by our laboratories using similar protein-interaction, cell-culture, brain-sample

and motor-behavior approaches. Subsequent power analysis was conducted for each parameter by using IBM SPSS software (IBM France, Bois-Colombes, France). The number of biological replicates (*e.g.*, number of mice, number of cell cultures) is provided in the corresponding figure legends. The number of technical replicates (*e.g.*, number of Y2H assays, number of incubations within each cell culture, number of sections microscopically analyzed per mouse brain, number of behavioral trials per mouse) is provided in the corresponding figure legends or in the corresponding Materials and Methods subsections. All the experiments conducted with animals are presented as dot plots. Graphs and statistics were generated by GraphPad Prism v8.0.1.

Results

BiP interacts with CB1R *in vitro*

To identify new CB1R-interacting intracellular proteins, we challenged the receptor's carboxyl-terminal domain (CTD; amino acids 408 to 472) to a cDNA library containing $>10^6$ different clones by means of a Y2H system. One particular cDNA clone, comprising amino acids 497 to 654 of the protein BiP (hereafter "BiP-interacting region"; BiP-IR), provided an unequivocally positive outcome (Fig. 1A). BiP, also known as GRP78 or Hspa5, belongs to the highly conserved Hsp70 family of molecular chaperones. These proteins consist of two different domains: an *N*-terminal nucleotide-binding domain (NBD) with ATPase activity, and a *C*-terminal substrate-binding domain (SBD). The SBD, in turn, is composed of a β-sandwich domain (SBDβ) and an α-helical lid (SBDα), which are interlinked by a hydrophobic stretch (Wieteska et al., 2017). It is generally believed that ATP-assisted, BiP-mediated protein refolding proceeds when hydrophobic peptides bind to a conserved groove in the SBDβ domain of BiP. Conversely, here, we found that CB1R-CTD interacts essentially with the lid domain in the absence of the groove. Specifically, according to the reported structures (Yang et al., 2015, 2017), BiP-IR would span the entire SBDα and two strands of the SBDβ (Fig. 1A, bottom diagram).

We next aimed to validate the molecular specificity of the interaction between CB1R-CTD and BiP-IR. First, by using directed Y2H assays, we delimitated the BiP-IR-binding site to a restricted 23 amino-acid stretch (residues 449-472) at the edge of CB1R-CTD (Fig. 1B). Second, we found that the CTD of CB2R, the GPCR with the highest sequence homology to CB1R, did not bind BiP-IR (Fig. 1B). Third, as the phosphorylation state of specific S and T residues in the CTD of a GPCR can determine its interaction with intracellular proteins, we challenged BiP-IR to every possible single

phosphomimetic mutant (S/T → D) within CB1R-CTD, and found that only the S452D point mutation, which is precisely located in the last 23 amino-acid portion of CB1R, impaired the association (Table 2). Fourth, we expressed recombinant CB1R-CTD, BiP-IR and BiP, and found that BiP and BiP-IR bind CB1R-CTD with a similar high affinity, as measured by fluorescence polarization-based protein-protein binding assays (Fig. 1C).

We subsequently conducted experiments in HEK-293T cells. First, co-immunoprecipitation studies showed that (*i*) CB1R-CTD, and specifically its 449-460 amino-acid stretch, was sufficient to bind BiP-IR (Fig. 1D); (*ii*) full-length CB1R also interacted with both BiP and BiP-IR (Fig. 1E); and (*iii*) BiP-IR exhibited little association with the S452D point-mutant of CB1R-CTD (Fig. 1F). Second, BRET experiments conducted with an Rluc-tagged version of CB1R also supported the protein-protein interaction (Fig. 1G, upper panel), and adding non-GFP-tagged versions of BiP as competitors decreased the BRET peak only when the BiP-IR was present (Fig. 1G, lower panel). Moreover, there was no overt binding between GFP-BiP-IR and CB1R-Rluc when the S452D single mutation was introduced in the receptor (Fig. 1G, upper panel).

Taken together, these data show that BiP interacts specifically with CB1R *in vitro*, both in purified-protein assays and in HEK-293T cells.

BiP modulates CB1R-evoked signaling

Dynamic mass redistribution (DMR) is a powerful tool to assess the overall signal triggered by the agonist-evoked activation of a particular receptor in living cells (Fang et al., 2007). In fact, we and others have previously used DMR to investigate CB1R-evoked signaling (Viñals et al., 2015; Moreno et al., 2018; Navarro et al., 2020). Here, by using HEK-293T cells expressing CB1R, we found a well-defined and saturating curve after

612 adding the cannabinoid receptor-selective agonist WIN-55,212-2 (Fig. 2A). Of note, co-
613 expression of full-length BiP led to a strong inhibition of CB1R signaling (Fig. 2A) but did
614 not alter the agonist-evoked response of two other $G_{i/o}$-coupled receptors (CB2R and
615 adenosine A_1 receptor) that were used as controls (Fig. 3A). The effect of BiP on CB1R
616 relied selectively on BiP-IR, as expressing this region rendered a comparable inhibition,
617 and no change was found with BiP-ΔIR (Fig. 2A). This effect was again subverted when
618 the S452D point mutation was inserted in CB1R (Fig. 3B), and was also evident –though
619 with a slower kinetics- when the endocannabinoids anandamide and 2-
620 arachidonoylglycerol) were used as receptor agonists (Fig. 2B). Given the similar
621 behavior of full-length BiP and BiP-IR, we used only BiP-IR for further signaling
622 experiments.
623 CB1R activation modulates multiple signaling pathways, being cAMP/PKA, ERK
624 and PI3K/Akt/mTORC1 the best characterized (Pertwee et al., 2010; Nogueras-Ortiz and
625 Yudowski, 2016). We thus aimed to dissect in detail the inhibitory effect of BiP-IR on
626 CB1R overall signaling observed in DMR assays. First, we found that BiP-IR did not alter
627 markedly the archetypical $G\alpha_{i/o}$-coupling profile of CB1R (Fig. 2C), nor affected the WIN-
628 55,212-2-evoked reduction of forskolin-augmented cAMP concentration (Fig. 2D). Next,
629 we analyzed the phosphorylation (activation) state of major cellular protein kinases by
630 using a phosphoprotein array. HEK-293T cells were transfected with the same
631 constructs used in the aforementioned DMR assays, and subsequently treated with
632 vehicle or WIN-55,212-2. Among the different pathways activated by the cannabinoid,
633 BiP-IR preferentially hampered the Akt/mTORC1 pathway (as inferred from Akt1/2/3-
634 T308, PRAS40-T246 and p70S6K-T389 phosphorylation) and the ERK pathway (as
635 inferred from ERK1/2-T202/Y204 phosphorylation) (Fig. 2E). The WIN-55,212-2-
636 mediated activation of CREB, an archetypical convergent substrate of the Akt/mTORC1

and ERK pathways, was also inhibited by BiP-IR (as inferred from CREB-S133 phosphorylation). We confirmed this BiP-mediated inhibition of CB1R-evoked signaling by analyzing pERK1/2-T202/Y204, pp70S6K-T389, and pCREB-S133 with conventional Western blotting (Fig. 2F). Accordingly, the PI3K inhibitor LY294002 and the MEK1 inhibitor U0126 blunted the WIN-55,212-2-evoked DMR signal (Fig. 3C).

To study how BiP selectively alters CB1R-mediated signaling independently of $G\alpha_{i/o}$ proteins, we evaluated the coupling of the receptor to non-$G\alpha_{i/o}$ G proteins. Of note, we found that CB1R also coupled to $G\alpha_{q/11}$, and this association was impaired by BiP-IR (Fig. 2G). Moreover, WIN-55,212-2-mediated ERK activation was mitigated by either pharmacological blockade of $G\alpha_{q/11}$ (with the drug YM-254890) or genetic interference of $G\alpha_{q/11}$ signaling (with a dominant-negative GFP-GRK2 construct) (Andradas et al., 2016) (Fig. 2H). Likewise, YM-254890 and dominant-negative $G\alpha_{q/11}$ reduced the WIN-55,212-2-evoked DMR response (Fig. 2I). We next analyzed the coupling of CB1R to $G\alpha_{q/11}$ in hippocampal extracts from adult $BiP^{+/-}$ (hereafter BiP-HET) and $BiP^{+/+}$ (hereafter BiP-WT) mice [Note that very early embryonic lethality occurs in $BiP^{-/-}$ mice (Luo et al., 2006).] In line with the aforementioned data from HEK-293T cells, CB1R showed a preference for $G\alpha_{q/11}$ coupling in BiP-HET mice compared to their BiP-WT littermates (Fig. 2J).

Taken together, these data show that BiP-IR affects CB1R-evoked signaling through the selective attenuation of an "alternative" $G\alpha_{q/11}$ protein-driven module, while leaving the "classical" $G\alpha_{i/o}$ protein-driven module essentially unaffected.

CB1R-BiP complexes reside on GABAergic terminals of the mouse brain

It is well established that CB1R resides largely on terminals of GABAergic neurons (Marsicano and Lutz, 1999; Katona and Freund, 2008). However, the precise neurochemical phenotype of BiP-expressing cells remains unclear (*cf.* Jin et al., 2018).

Hence, we analyzed the expression of BiP mRNA in GABAergic *vs.* glutamatergic neurons by *in situ* hybridization histochemistry. BiP mRNA was localized throughout the mouse brain (Fig. 4A), showing a more ubiquitous expression pattern than CB1R mRNA (Fig. 4B). Of note, nearly all the hippocampal high CB1R mRNA-expressing cells were also positive for BiP mRNA [93.7 ± 1.7% in the CA1/3 areas and 94.6 ± 3.4% in the dentate gyrus (DG)] (Figs. 4C and 4D). In the CA1/3 hippocampal areas, as reported for CB1R mRNA (Marsicano and Lutz, 1999), BiP mRNA showed a high co-localization with GAD65/67 mRNA (81.6 ± 4.4% of the BiP-positive cells co-expressed GAD65/67) (Figs. 5A and 5B), while co-localization with vGluT1 mRNA was hardly detectable in the scattered BiP-expressing cells adjacent to the BiP/vGluT1 mRNA-enriched pyramidal cell layer (<1% of the BiP-positive cells co-expressed vGluT1) (Figs. 5C and 5D). In the DG, the distribution of BiP mRNA between disseminated GAD65/67 mRNA-expressing neurons (Figs. 5A and 5B) and vGluT1 mRNA-expressing neurons (Figs. 5C and 5D) was more balanced, although again with a preference towards inhibitory cells (47.0 ± 9.9% and 30.0 ± 7.2% of the BiP-positive cells co-expressed GAD65/67 or vGluT1, respectively).

The most widely reported subcellular localization of BiP is the endoplasmic reticulum (ER) lumen, while CB1R is largely located at the plasma membrane, and its CTD faces the cytoplasm since its biosynthesis starts on the ER. To assess this apparent inconsistency, we performed subcellular fractionation experiments in mouse brain samples. Analysis of hippocampal, striatal, and cortical tissue extracts showed that BiP is present not only in the ER but also in the cytosolic fraction (Figs. 6A and 6B). This observation supports the notion that cytoplasmic BiP binds to CB1R-CTD, and aligns with previous reports showing that not all BiP functions can be attributed to its interaction with ER-resident proteins (Belfi et al., 1999; Cha-Molstad et al., 2015; Shim et al., 2018;

687 Yoon et al., 2018), and that a population of BiP molecules is found adjacent to the
688 plasma membrane (Tsai et al., 2015). As the majority of CB1R resides at the
689 presynapse, where it controls neurotransmitter release (Piomelli, 2003), we also
690 evaluated whether CB1R-BiP complexes are present in this subcellular location. PLA
691 analyses revealed a pronounced positive signal in synaptosomes from the hippocampus,
692 striatum, and cortex of CB1R-WT mice, but not of CB1R-KO littermates (Fig. 6C).
693 Next, to obtain a detailed neuroanatomical map of CB1R-BiP protein complexes,
694 we conducted *in situ* PLA assays on brain slices from various genetic mouse models of
695 conditional loss or gain of CB1R expression (Fig. 7A). We first used hippocampi from
696 conditional CB1R-KO models (Marsicano et al., 2002) (Figs. 7B, 7D, 7E and 7G). PLA
697 experiments conducted on hippocampal sections from control adult $CB1R^{floxed/floxed}$
698 (hereafter CB1R-floxed) mice showed that 63.2 ± 4.7% and 62.9 ± 11.2% of the cells
699 contained positive *puncta* in the DG and CA1, respectively. This signal was strongly
700 reduced in sections from $CB1R^{floxed/floxed;CMV-Cre}$ (hereafter CB1R-KO) mice (DG: 14.8 ±
701 5.0%; CA1: 18.8 ± 4.5%). In conditional knockout mice in which the gene encoding
702 CB1R had been selectively deleted from forebrain GABAergic neurons
703 ($CB1R^{floxed/floxed;Dlx5/6-Cre}$; hereafter GABA-CB1R-KO), we found a notable decrease in the
704 percentage of cells expressing positive dots (DG: 31.9 ± 6.2%; CA1: 33.9 ± 7.8%). In
705 contrast, sections from mice in which the gene encoding CB1R had been selectively
706 deleted from dorsal telencephalic glutamatergic neurons ($CB_1R^{floxed/floxed;Nex1-Cre}$; hereafter
707 Glu-CB1R-KO) displayed a similar pattern of PLA staining than their CB1R-floxed
708 counterparts (DG: 58.6 ± 5.9%; CA1: 60.8 ± 1.1%). Comparable overall data were
709 obtained in sections from mouse striatum and cortex (Figs. 8A, 8B, 8D, 8E and 8G).
710 We subsequently made use of a Cre-mediated, lineage-specific, CB1R gene
711 expression-rescue strategy from a CB1R-null background (hereafter Stop-CB1R mice)

712 (De Salas-Quiroga et al., 2015; De Giacomo et al., 2020a) (Figs. 7C, 7D, 7F and 7G).
713 PLA assays in hippocampal sections from these mice showed, as expected, a marginal
714 CB1R-KO-like background signal (DG: 20.1 ± 3.2%; CA1: 21.2 ± 3.2%). In line with the
715 data from conditional knockout mice, rescuing CB1R gene expression with a constitutive
716 Cre recombinase (Stop-CB1R$^{EIIa\text{-}Cre}$, hereafter, CB1R-RS) restored CB1R-BiP
717 complexes to the levels of control CB1R-floxed mice (DG: 59.6 ± 5.5%; CA1: 58.5 ±
718 5.8%). This effect was paralleled in brain sections from conditionally-rescued Stop-
719 CB1R$^{Dlx5/6\text{-}Cre}$ (hereafter, GABA-CB1R-RS) mice (DG: 58.1 ± 9.6%; CA1: 56.9 ± 5.5%)
720 but not from conditionally-rescued Stop-CB1R$^{Nex1\text{-}Cre}$ (hereafter, Glu-CB1R-RS) mice
721 (DG: 21.1 ± 3.2%; CA1: 20.0 ± 2.5%). As in the aforementioned conditional knockout
722 mouse experiments, these CB1R gene expression-rescue data in the mouse
723 hippocampus displayed a similar global pattern in the striatum and cortex (Figs. 8C, 8D,
724 8F and 8G).
725 Taken together, these data support the interaction between CB1R and BiP in
726 three key regions of the mouse brain, and, more specifically, a restricted occurrence of
727 CB1R-BiP complexes in GABAergic neurons.
728
729 **BiP affects CB1R function *in vivo***
730 THC induces numerous behavioral changes in laboratory animals and humans. The
731 combination of hypolocomotion, analgesia, catalepsy and hypothermia, usually
732 designated as the “cannabinoid tetrad”, has evolved as a powerful tool to identify
733 pharmacological or genetic interventions that target CB1R (Martin, 1986; Metna-Laurent
734 et al., 2017). Previous studies have shown that these four behavioral traits rely
735 selectively on the activation of CB1R molecules located on various populations of
736 glutamatergic or dopamine D_1 receptor-expressing projection neurons, but not on

737 GABAergic interneurons, thus allowing a neurobiological correlate between CB1R
738 cellular expression and function (Monory et al., 2007; De Giacomo et al., 2020a). We
739 studied the “cannabinoid tetrad” in BiP-HET and BiP-WT littermates (Fig. 9A), and found
740 that acute THC injection (10 mg/kg, i.p.) elicited the four archetypical effects of the
741 “cannabinoid tetrad” to the same extent in BiP-HET and BiP-WT animals (Fig. 9, left
742 panels). In addition, following a 5-day sustained treatment, BiP-HET and BiP-WT mice
743 developed a comparable tolerance to THC (Fig. 9, right panels).
744 As the CB1R-BiP complexes reside selectively on GABAergic neurons (see
745 above), it is not surprising that the deletion of a BiP allele does not modify any of the
746 classical “cannabinoid tetrad” behavioral traits. Of note, anxiety-like behaviors induced
747 by cannabinoid intoxication have been shown to rely selectively on the activation of
748 CB1R molecules located on GABAergic interneurons (Rey et al., 2012; De Giacomo et
749 al., 2020a, 2020b). Because the open-field test of the “cannabinoid tetrad” can also be
750 used to define anxious phenotypes by evaluating the relative ambulation of the animals
751 across the center of the arena (Seibenhener and Wooten, 2015), we conducted these
752 analyses in our experimental setting. A single THC injection reduced the ambulation of
753 the mice across the center of the arena equally in BiP-HET and BiP-WT mice (Fig. 10A,
754 left panel). However, after a 5-day continuing THC treatment, the ambulation across the
755 centre of the arena remained lowered by acute THC in BiP-HET mice but not in their
756 BiP-WT littermates (Fig. 10A, right panel).
757 To provide further support to the control of CB1R-mediated anxiety by BiP, we
758 used the elevated plus maze test, a widely recognized measure of anxiety that served
759 originally to define the anxiogenic activity of the CB1R pool located on GABAergic
760 neurons (Rey et al., 2012). We injected BiP-WT and BiP-HET mice with vehicle or THC
761 (10 mg/kg, i.p.), and found that the drug induced only an anxiogenic trend in BiP-WT

762 mice but a significant anxiogenic effect in BiP-HET littermates, as evidenced by the
763 decrease in both the number of entries (Fig. 10B, left panel) and the time of permanence
764 (Fig. 10B, right panel) in the open arms of the device.

765 Taken together, these data support that BiP, by interacting with CB1R on
766 GABAergic neurons, modulates anxiety-like behaviors upon cannabinoid administration.

767

Discussion

Here, we show that BiP interacts specifically with CB1R-CTD. BiP is known to interact with some GPCRs during their folding (Siffroi-Fernandez et al., 2002; Mizrachi and Segaloff, 2004; Langer et al., 2008), and has been found associated to melanocortin MC_4 receptors at the plasma membrane (Yoon et al., 2018). The CB1R-BiP interaction occurs between a short amino-acid stretch in the CB1R-CTD and the BiP-SBDα domain. The latter domain, to our knowledge, has never been implicated in the binding of BiP to membrane receptors. As the protein-binding/refolding function of BiP is usually ascribed to its SBDβ domain (Yang et al., 2015, 2017), we cannot rule out that additional proteins interact through this region onto the CB1R-BiP complexes. The BiP-interacting region in CB1R partially overlaps with the putative *C*-terminal helix 9 of the receptor (Ahn et al., 2009), which might serve as an axon-targeting signal and a potential protein-protein interaction site (Fletcher-Jones et al., 2019). How the synaptic trafficking of CB1R could be controlled by BiP is therefore an intriguing possibility that remains to be explored. Additionally, the BiP-binding region of CB1R contains a specific phosphorylation site (S452) that regulates this protein-protein interaction, and may conceivably participate in agonist-induced receptor signaling and subsequent internalization (Daigle et al., 2008). In fact, a high-throughput phosphoproteomic study identified this phosphorylated residue in the mouse brain (Wiśniewski et al., 2010). The lack of reported mutations in this BiP-binding region of CB1R (https://gpcrdb.org), along with its evolutionary conservation, further supports its biological importance.

CB1R-evoked signaling is markedly affected upon BiP binding. This finding contrasts with the subtle effect of CRIP1a on CB1R/G-protein coupling (Blume et al., 2015), and with the BiP-mediated facilitation of melanocortin MC_4 receptor activation (Yoon et al., 2018). Accruing evidence has linked ERK and Akt/mTORC1 activation to

various key CB1R-evoked effects in the brain (Rubino et al., 2007; Guegan et al., 2013; Puighermanal et al., 2013; Blázquez et al., 2020). However, the possible relevance of $G\alpha_{q/11}$ protein in CB1R neurobiological action remains unclear (Diez-Alarcia et al., 2016). Our data unveil an unprecedented functional coupling of CB1R signaling to $G\alpha_{q/11}$, as well as a selective hampering effect of BiP on it. Interestingly, regions analogous to CB1R helix 9, which overlaps with the BiP-binding site, have been reported to act as $G\alpha_{q/11}$-binding sites in rhodopsin (Murakami and Kouyama, 2008) and bradykinin B_2 receptor (Piserchio et al., 2005). Thus, it is conceivable that in CB1R the binding of BiP constitutes a competitive steric impediment to achieve $G\alpha_{q/11}$ binding and activation.

Our detailed mapping of CB1R-BiP complexes in the mouse brain shows that GABAergic neurons constitute the foremost cell population expressing these complexes. This is in line with a previous high-throughput proteomic study showing that BiP co-immunoprecipitates with CB1R in mouse GABAergic neurons (Mattheus et al., 2016). It is worth noting that, despite their low CB1R/G-protein coupling efficacy (Steindel et al., 2013), GABAergic terminals contain large amounts of CB1R (Marsicano and Lutz, 1999; Katona and Freund, 2008) likely displaying a high tonic activity (Roberto et al., 2010). Given its inhibitory role, we speculate that BiP binding may represent a counterpoint to ensure a balanced CB1R activity in the physiological control of glutamatergic/GABAergic neurotransmission. More specifically, THC-elicited anxiety relies on mTORC1 activation upon engagement of CB1R on hippocampal GABAergic interneurons (Rey et al., 2012; Puighermanal et al., 2013; De Giacomo et al., 2020a, 2020b). In addition, a role of $G\alpha_{q/11}$ protein-coupled receptors (*e.g.*, serotonin 5-HT_{2C} receptor) in the induction of anxiety has been suggested (Mazzone et al., 2018). Thus, we propose that the THC-evoked high-input activation of a restricted $G\alpha_{q/11}$-coupled pool of CB1R molecules located on hippocampal GABAergic interneurons, *via* the mTORC1 signaling axis, triggers anxiety-

like behaviors, a process plausibly controlled by BiP binding to CB1R at the presynapse. This would provide an unprecedented mechanism for the spatially-selective control of CB1R signaling in the brain, and supports that favoring CB1R-BiP association would reduce anxiety, a frequent negative effect of CB1R over-activation. As CB1R-BiP complexes also reside on GABAergic neurons in other brain regions as the cortex and striatum, the possibility that BiP binding controls additional CB1R-related behaviors remains to be determined.

826 **References**

827 Abrams DI (2018) The therapeutic effects of Cannabis and cannabinoids: An update
828 from the National Academies of Sciences, Engineering and Medicine report. Eur J
829 Intern Med 49:7–11.
830 Ahn KH, Pellegrini M, Tsomaia N, Yatawara AK, Kendall DA, Mierke DF (2009)
831 Structural analysis of the human cannabinoid receptor one carboxyl-terminus
832 identifies two amphipathic helices. Biopolymers 91:565–573.
833 Andradas C et al. (2016) Activation of the orphan receptor GPR55 by
834 lysophosphatidylinositol promotes metastasis in triple-negative breast cancer.
835 Oncotarget 7:47565–47575.
836 Belfi CA, Chatterjee S, Gosky DM, Berger SJ, Berger NA (1999) Increased sensitivity of
837 human colon cancer cells to DNA cross-linking agents after GRP78 up-regulation.
838 Biochem Biophys Res Commun 257:361–368.
839 Bellocchio L, Lafentre P, Cannich A, Cota D, Puente N, Grandes P, Chaouloff F, Piazza
840 PV, Marsicano G (2010) Bimodal control of stimulated food intake by the
841 endocannabinoid system. Nat Neurosci 13:281–283.
842 Blázquez C, Ruiz-Calvo A, Bajo-Grañeras R, Baufreton JM, Resel E, Varilh M, Pagano
843 Zottola AC, Mariani Y, Cannich A, Rodríguez-Navarro JA, Marsicano G, Galve-
844 Roperh I, Bellocchio L, Guzmán M (2020) Inhibition of striatonigral autophagy as a
845 link between cannabinoid intoxication and impairment of motor coordination. Elife
846 9: e56811.
847 Blume LC, Eldeeb K, Bass CE, Selley DE, Howlett AC (2015) Cannabinoid receptor
848 interacting protein (CRIP1a) attenuates CB1R signaling in neuronal cells. Cell
849 Signal 27:716–726.
850 Cha-Molstad H et al. (2015) Amino-terminal arginylation targets endoplasmic reticulum

851 chaperone BiP for autophagy through p62 binding. Nat Cell Biol 17:917–929.
852 Daigle TL, Kwok ML, Mackie K (2008) Regulation of CB_1 cannabinoid receptor
853 internalization by a promiscuous phosphorylation-dependent mechanism. J
854 Neurochem 106:70–82.
855 De Giacomo V, Ruehle S, Lutz B, Häring M, Remmers F (2020a) Differential
856 glutamatergic and GABAergic contributions to the tetrad effects of Δ^9-
857 tetrahydrocannabinol revealed by cell-type-specific reconstitution of the CB_1
858 receptor. Neuropharmacology 179:108287.
859 De Giacomo V, Ruehle S, Lutz B, Häring M, Remmers F (2020b) Cell type-specific
860 genetic reconstitution of CB1 receptor subsets to assess their role in exploratory
861 behaviour, sociability and memory. Eur J Neurosci. Online ahead of print.
862 De Salas-Quiroga A, Díaz-Alonso J, García-Rincón D, Remmers F, Vega D, Gómez-
863 Cañas M, Lutz B, Guzmán M, Galve-Roperh I (2015) Prenatal exposure to
864 cannabinoids evokes long-lasting functional alterations by targeting CB_1 receptors
865 on developing cortical neurons. Proc Natl Acad Sci USA 112:13693–13698.
866 Diez-Alarcia R, Ibarra-Lecue I, Lopez-Cardona ÁP, Meana J, Gutierrez-Adán A, Callado
867 LF, Agirregoitia E, Urigüen L (2016) Biased agonism of three different cannabinoid
868 receptor agonists in mouse brain cortex. Front Pharmacol 7:1–13.
869 Dudok B et al. (2015) Cell-specific STORM super-resolution imaging reveals nanoscale
870 organization of cannabinoid signaling. Nat Neurosci 18:75–86.
871 Fang Y, Li G, Ferrie AM (2007) Non-invasive optical biosensor for assaying endogenous
872 G protein-coupled receptors in adherent cells. J Pharmacol Toxicol Methods
873 55:314–322.
874 Fernández-Ruiz J (2019) The biomedical challenge of neurodegenerative disorders: an
875 opportunity for cannabinoid-based therapies to improve on the poor current

876 therapeutic outcomes. Br J Pharmacol 176:1370–1383.
877 Fletcher-Jones A, Hildick KL, Evans AJ, Nakamura Y, Wilkinson KA, Henley JM (2019)
878 The C-Terminal helix 9 motif in rat cannabinoid receptor type 1 regulates axonal
879 trafficking and surface expression. Elife 8:1–26.
880 García-Nafría J, Watson JF, Greger IH (2016) IVA cloning: A single-tube universal
881 cloning system exploiting bacterial In Vivo Assembly. Sci Rep 6:1–12.
882 Guegan T, Cutando L, Gangarossa G, Santini E, Fisone G, Martinez A, Valjent E,
883 Maldonado R, Martin M (2013) Operant behavior to obtain palatable food modifies
884 ERK activity in the brain reward circuit. Eur Neuropsychopharmacol 23:240–252.
885 Guggenhuber S, Alpar A, Chen R, Schmitz N, Wickert M, Mattheus T, Harasta AE,
886 Purrio M, Kaiser N, Elphick MR, Monory K, Kilb W, Luhmann HJ, Harkany T, Lutz
887 B, Klugmann M (2016) Cannabinoid receptor-interacting protein Crip1a modulates
888 CB_1 receptor signaling in mouse hippocampus. Brain Struct Funct:2061–2074.
889 Hill KP (2015) Medical marijuana for treatment of chronic pain and other medical and
890 psychiatric problems: A clinical review. JAMA 313:2474–2483.
891 Howlett A, Blume L, Dalton G (2010) CB_1 cannabinoid receptors and their associated
892 proteins. Curr Med Chem 17:1382–1393.
893 Jin X, Kim DK, Riew T-R, Kim HL, Lee M-Y (2018) Cellular and subcellular localization of
894 endoplasmic reticulum chaperone GRP78 following transient focal cerebral
895 ischemia in rats. Neurochem Res 43:1348–1362.
896 Katona I, Freund TF (2008) Endocannabinoid signaling as a synaptic circuit breaker in
897 neurological disease. Nat Med 14:923–930.
898 Langer I, Leroy K, Gaspard N, Brion JP, Robberecht P (2008) Cell surface targeting of
899 VPAC1 receptors: Evidence for implication of a quality control system and the
900 proteasome. Biochim Biophys Acta 1783:1663–1672.

901 Lauckner JE, Hille B, Mackie K (2005) The cannabinoid agonist WIN55,212-2 increases
902 intracellular calcium via CB_1 receptor coupling to $G_{q/11}$ G proteins. Proc Natl Acad
903 Sci USA 102:19144–19149.
904 Luo S, Mao C, Lee B, Lee AS (2006) GRP78/BiP is required for cell proliferation and
905 protecting the inner cell mass from apoptosis during early mouse embryonic
906 development. Mol Cell Biol 26:5688–5697.
907 Magalhaes AC, Dunn H, Ferguson SSG (2012) Regulation of GPCR activity, trafficking
908 and localization by GPCR-interacting proteins. Br J Pharmacol 165:1717–1736.
909 Marsicano G, Lutz B (1999) Expression of the cannabinoid receptor CB1 in distinct
910 neuronal subpopulations in the adult mouse forebrain. Eur J Neurosci 11:4213–
911 4225.
912 Marsicano G, Wotjak CT, Azad SC, Bisogno T, Rammes G, Cascioll MG, Hermann H,
913 Tang J, Hofmann C, Zieglgänsberger W, Di Marzo V, Lutz B (2002) The
914 endogenous cannabinoid system controls extinction of aversive memories. Nature
915 418:530–534.
916 Martin BR (1986) Cellular effects of cannabinoids. Pharmacol Rev 38:45–74.
917 Mattheus T, Kukla K, Zimmermann T, Tenzer S, Lutz B (2016) Cell type-specific tandem
918 affinity purification of the mouse hippocampal CB_1 receptor-associated proteome. J
919 Proteome Res 15:3585–3601.
920 Maurice P, Guillaume J-L, Benleulmi-Chaachoua A, Daulat AM, Kamal M, Jockers R
921 (2011) GPCR-interacting proteins, major players of GPCR function. Adv Pharmacol
922 62:349–380.
923 Mazzone CM, Pati D, Michaelides M, DiBerto J, Fox JH, Tipton G, Anderson C, Duffy K,
924 McKlveen JM, Hardaway JA, Magness ST, Falls WA, Hammack SE, McElligott ZA,
925 Hurd YL, Kash TL (2018) Acute engagement of Gq-mediated signaling in the bed

926 nucleus of the stria terminalis induces anxiety-like behavior. Mol Psychiatry 23:143–
927 153.
928 Mechoulam R, Hanuš LO, Pertwee R, Howlett AC (2014) Early phytocannabinoid
929 chemistry to endocannabinoids and beyond. Nat Rev Neurosci 15:757–764.
930 Mechoulam R, Parker LA (2013) The endocannabinoid system and the brain. Annu Rev
931 Psychol 64:21–47.
932 Merino-Gracia J, Costas-Insua C, Ángeles Canales M, Rodríguez-Crespo I (2016a)
933 Insights into the C-terminal peptide binding specificity of the PDZ domain of
934 neuronal nitric-oxide synthase: Characterization of the interaction with the tight
935 junction protein claudin-3. J Biol Chem 291:11581–11595.
936 Merino-Gracia J, Zamora-Carreras H, Bruix M, Rodríguez-Crespo I (2016b) Molecular
937 basis for the protein recognition specificity of the dynein light chain DYNLT1/Tctex1:
938 Characterization of the interaction with activin receptor IIB. J Biol Chem 291:20962–
939 20975.
940 Metna-Laurent M, Mondésir M, Grel A, Vallée M, Piazza PV (2017) Cannabinoid-
941 induced tetrad in mice. Curr Protoc Neurosci 2017:9.59.1-9.59.10.
942 Mizrachi D, Segaloff DL (2004) Intracellularly located misfolded glycoprotein hormone
943 receptors associate with different chaperone proteins than their cognate wild-type
944 receptors. Mol Endocrinol 18:1768–1777.
945 Monory K et al. (2006) The endocannabinoid system controls key epileptogenic circuits
946 in the hippocampus. Neuron 51:455–466.
947 Monory K, Blaudzun H, Massa F, Kaiser N, Lemberger T, Schütz G, Wotjak CT, Lutz B,
948 Marsicano G (2007) Genetic dissection of behavioural and autonomic effects of Δ^9-
949 tetrahydrocannabinol in mice. PLoS Biol 5:e269.
950 Moreno E et al. (2018) Singular location and signaling profile of adenosine A_{2A}-

951 cannabinoid CB_1 receptor heteromers in the dorsal striatum.
952 Neuropsychopharmacology 43:964–977.
953 Murakami M, Kouyama T (2008) Crystal structure of squid rhodopsin. Nature 453:363–
954 367.
955 Navarro G, Varani K, Lillo A, Vincenzi F, Rivas-Santisteban R, Raïch I, Reyes-Resina I,
956 Ferreiro-Vera C, Borea PA, Sánchez de Medina V, Nadal X, Franco R (2020)
957 Pharmacological data of cannabidiol- and cannabigerol-type phytocannabinoids
958 acting on cannabinoid CB_1, CB_2 and CB_1/CB_2 heteromer receptors. Pharmacol Res
959 159:104940.
960 Nogueras-Ortiz C, Yudowski GA (2016) The multiple waves of cannabinoid 1 receptor
961 signaling. Mol Pharmacol 90:620–626.
962 Pertwee RG, Howlett AC, Abood ME, Alexander SPH, Di Marzo V, Elphick MR,
963 Greasley PJ, Hansen HS, Kunos G, Mackie K, Mechoulam R, Ross RA (2010)
964 International Union of Basic and Clinical Pharmacology. LXXIX. Cannabinoid
965 receptors and their ligands: beyond CB_1 and CB_2. Pharmacol Rev 62:588–631.
966 Piomelli D (2003) The molecular logic of endocannabinoid signalling. Nat Rev Neurosci
967 4:873–884.
968 Piserchio A, Zelesky V, Yu J, Taylor L, Polgar P, Mierke DF (2005) Bradykinin B2
969 receptor signaling: Structural and functional characterization of the C-terminus.
970 Biopolymers 80:367–373.
971 Priestley R, Glass M, Kendall D (2017) Functional selectivity at cannabinoid receptors.
972 Adv Pharmacol 80:207–221.
973 Puighermanal E, Busquets-Garcia A, Gomis-González M, Marsicano G, Maldonado R,
974 Ozaita A (2013) Dissociation of the pharmacological effects of THC by mTOR
975 blockade. Neuropsychopharmacology 38:1334–1343.

Rey AA, Purrio M, Viveros MP, Lutz B (2012) Biphasic effects of cannabinoids in anxiety responses: CB1 and GABA B receptors in the balance of gabaergic and glutamatergic neurotransmission. Neuropsychopharmacology 37:2624–2634.

Reyes-Irisarri E, Sanchez AJ, Garcia-Merino JA, Mengod G (2007) Selective induction of cAMP phosphodiesterase PDE4B2 expression in experimental autoimmune encephalomyelitis. J Neuropathol Exp Neurol 66:923-931.

Roberto M, Cruz M, Bajo M, Siggins GR, Parsons LH, Schweitzer P (2010) The endocannabinoid system tonically regulates inhibitory transmission and depresses the effect of ethanol in central amygdala. Neuropsychopharmacology 35:1962–1972.

Rubino T, Sala M, Viganò D, Braida D, Castiglioni C, Limonta V, Guidali C, Realini N, Parolaro D (2007) Cellular mechanisms underlying the anxiolytic effect of low doses of peripheral delta-9-tetrahydrocannabinol in rats. Neuropsychopharmacology 32:2036–2045.

Ruehle S, Remmers F, Romo-Parra H, Massa F, Wickert M, Wörtge S, Häring M, Kaiser N, Marsicano G, Pape HC, Lutz B (2013) Cannabinoid CB_1 receptor in dorsal telencephalic glutamatergic neurons: Distinctive sufficiency for hippocampus-dependent and amygdala-dependent synaptic and behavioral functions. J Neurosci 33:10264–10277.

Ruiz-Calvo A, Maroto IB, Bajo-Grañeras R, Chiarlone A, Gaudioso Á, Ferrero JJ, Resel E, Sánchez-Prieto J, Rodríguez-Navarro JA, Marsicano G, Galve-Roperh I, Bellocchio L, Guzmán M (2018) Pathway-specific control of striatal neuron vulnerability by corticostriatal cannabinoid CB_1 receptors. Cereb Cortex 28:307–322.

Sanabra C, Mengod G (2011) Neuroanatomical distribution and neurochemical

characterization of cells expressing adenylyl cyclase isoforms in mouse and rat brain. J Chem Neuroanat 41:43-54.

Seibenhener ML, Wooten MC (2015) Use of the open field maze to measure locomotor and anxiety-like behavior in mice. J Vis Exp:52434.

Shim SM, Choi HR, Sung KW, Lee YJ, Kim ST, Kim D, Mun SR, Hwang J, Cha-Molstad H, Ciechanover A, Kim BY, Kwon YT (2018) The endoplasmic reticulum-residing chaperone BiP is short-lived and metabolized through N-terminal arginylation. Sci Signal 11: eaan0630.

Siffroi-Fernandez S, Giraud A, Lanet J, Franc JL (2002) Association of the thyrotropin receptor with calnexin, calreticulin and BiP: Effects on the maturation of the receptor. Eur J Biochem 269:4930–4937.

Steindel F, Lerner R, Häring M, Ruehle S, Marsicano G, Lutz B, Monory K (2013) Neuron-type specific cannabinoid-mediated G protein signalling in mouse hippocampus. J Neurochem 124:795–807.

Tsai YL, Zhang Y, Tseng CC, Stanciauskas R, Pinaud F, Lee AS (2015) Characterization and mechanism of stress-induced translocation of 78-kilodalton glucose-regulated protein (GRP78) to the cell surface. J Biol Chem 290:8049–8064.

Velasco G, Sánchez C, Guzmán M (2012) Towards the use of cannabinoids as antitumour agents. Nat Rev Cancer 12:436–444.

Viñals X, Moreno E, Lanfumey L, Cordomí A, Pastor A, de La Torre R, Gasperini P, Navarro G, Howell LA, Pardo L, Lluís C, Canela EI, McCormick PJ, Maldonado R, Robledo P (2015) Cognitive impairment induced by delta9-tetrahydrocannabinol occurs through heteromers between cannabinoid CB_1 and serotonin 5-HT_{2A} Receptors. PLoS Biol 13:e1002194.

Wheeler D, Sneddon WB, Wang B, Friedman PA, Romero G (2007) NHERF-1 and the

cytoskeleton regulate the traffic and membrane dynamics of G protein-coupled receptors. J Biol Chem 282:25076–25087.

Wieteska L, Shahidi S, Zhuravleva A (2017) Allosteric fine-tuning of the conformational equilibrium poises the chaperone BiP for post-translational regulation. Elife 6:1–20.

Wiśniewski JR, Nagaraj N, Zougman A, Gnad F, Mann M (2010) Brain phosphoproteome obtained by a fasp-based method reveals plasma membrane protein topology. J Proteome Res 9:3280–3289.

Yang J, Nune M, Zong Y, Zhou L, Liu Q (2015) Close and allosteric opening of the polypeptide-binding site in a human Hsp70 chaperone BiP. Structure 23:2191–2203.

Yang J, Zong Y, Su J, Li H, Zhu H, Columbus L, Zhou L, Liu Q (2017) Conformation transitions of the polypeptide-binding pocket support an active substrate release from Hsp70s. Nat Commun 8:1202.

Yoon YR, Lee TG, Choi MH, Shin SW, Ko YG, Rhyu IJ, Kim DH, Seong JK, Baik JH (2018) Glucose-regulated protein 78 binds to and regulates the melanocortin-4 receptor. Exp Mol Med 50:1–14.

Figure legends

Figure 1. BiP interacts with CB1R *in vitro*

A, Scheme of the Y2H experiment using CB1R-CTD (amino acids 408-472) as bait and a human cDNA library (>10^6 clones) as prey. One cDNA clone (stained in blue) contained BiP/GRP78/Hspa5 amino acids 497-654 (BiP-IR). A diagram depicting the main structural domains of BiP/GRP78/Hspa5 is shown. **B,** Scheme of the Y2H experiment using fragments of CB1R-CTD or CB2R-CTD as bait and BiP-IR as prey. **C,** Fluorescence polarization-based protein-protein binding experiments using 5-IAF-labeled CB1R-CTD and increasing amounts of unlabeled BiP (upper panel) or BiP-IR (lower panel). A representative experiment, including the gels of the purified proteins, is shown (n=3). **D,** Co-immunoprecipitation experiments in HEK-293T cells expressing fragments of GFP-CB1R-CTD and 3xFLAG-BiP-IR. Immunoprecipitation (IP) was conducted with anti-GFP antibody. WCL: whole-cell lysate. A representative experiment is shown (n=3). **E,** Co-immunoprecipitation experiments in HEK-293T cells expressing HA-CB1R and 3xFLAG-BiP or 3xFLAG-BiP-IR. IP was conducted with anti-HA antibody (left panel) or anti-FLAG antibody (right panel). The asterisk denotes immunoglobulin heavy and light chains. A representative experiment is shown (n=3). **F,** Co-immunoprecipitation experiments in HEK-293T cells expressing GFP-CB1R-CTD wild-type or an S452D point-mutant form, along with 3xFLAG-BiP-IR. IP was conducted with anti-GFP antibody. A representative experiment is shown (n=3). **G,** BRET experiments in HEK-293T cells expressing CB1R-Rluc or CB1R-S452D-Rluc and increasing amounts of GFP-BiP-IR (upper panel; a representative experiment is shown; n=3), together or not with non-tagged versions of BiP, BiP-IR or BiP-ΔIR as competitors (lower panel). $^{**}p<0.01$ from control vector by one-way ANOVA with Tukey's multiple comparisons test

(n=3).

Figure 2. BiP modulates CB1R-evoked signaling

A, DMR experiments in HEK-293T cells expressing CB1R, together or not with BiP, BiP-IR or BiP-ΔIR, and incubated with vehicle or WIN-55,212-2 (100 nM). A representative experiment is shown (n=3). **B,** DMR experiments in HEK-293T cells expressing CB1R, together or not with BiP-IR, and incubated with vehicle or endocannabinoid (10 µM; 2-AG, 2-arachidonoylglycerol; AEA, anandamide). A representative experiment is shown (n=3). **C,** Coupling of CB1R to $G\alpha_{i/o}$ proteins in membrane extracts from HEK-293T cells expressing CB1R, together or not with BiP-IR. **p*<0.05 from basal (dashed line), or $^{\#}p$<0.05 from control vector, by one-sample Student's *t*-test or unpaired Student's *t*-test, respectively (n=3). **D,** cAMP concentration in HEK-293T cells expressing CB1R, together or not with BiP-IR. Cells were incubated first for 15 min with vehicle or WIN-55,212-2 (100 nM), and then for 15 min with vehicle or forskolin (FSK; 500 nM). ***p*<0.01 from vehicle, or $^{\#\#}p$<0.01 from FSK alone, by two-way ANOVA with Tukey's multiple comparisons test (n=3). **E,** HEK-293T cells expressing CB1R, together or not with BiP-IR, were incubated for 5 or 15 min with vehicle or WIN-55,212-2 (100 nM), and cell extracts were blotted on a phosphoprotein array. Two different times of membrane exposure are shown to allow an appropriate visualization of the main proteins affected (framed spots). A representative experiment is shown (n=2; membranes from vehicle-treated cells are omitted for clarity). The heat map represents values of mean fold-activation by WIN-55,212-2 over vehicle. **F,** Validation of some of the phosphoarray hits by conventional Western blotting in the same cell extracts used in panel D. A representative experiment is shown (n=2). **G,** Coupling of CB1R to non-$G\alpha_{i/o}$ Gα proteins in membrane extracts from HEK-293T cells expressing CB1R, together or not with BiP-

IR. *p<0.05 from basal (dashed line), or $^{\#}p$<0.05 from control vector, by one-sample Student's *t*-test or unpaired Student's *t*-test, respectively (n=3). **H,** Western blotting of phospho-ERK in HEK-293T cells expressing CB1R, and incubated for 5, 10 or 15 min with vehicle or WIN-55,212-2 (100 nM). Upper panel: Cells were pre-incubated for 30 min with vehicle or YM-254890 (1 µM). Lower panel: Cells co-expressed control vector (GFP) or $G\alpha_{q/11}$ dominant-negative vector (GFP-GRK2). A representative experiment is shown (n=3). **I,** DMR experiments in HEK-293T cells expressing CB1R under the same experimental conditions as in panel G. A representative experiment is shown (n=3). **J,** Coupling of CB1R to $G\alpha_{q/11}$ protein in hippocampal extracts from 3–4-month-old $BiP^{+/+}$ (BiP-WT) and $BiP^{+/-}$ (BiP-HET) mice. *p<0.05 from basal (dashed line), or $^{\#}p$<0.05 from BiP-WT group, by one-sample Student's *t*-test or unpaired Student's *t*-test, respectively (n=5-6 mice per group).

Figure 3. Controls of specificity of the CB1R-BiP DMR experiments

A, DMR experiments in HEK-293T cells expressing CB2R, together or not with BiP, and incubated with vehicle or the CB2R-selective agonist HU-308 (100 nM); or in HEK-293T cells expressing A1R, together or not with BiP, and incubated with vehicle or the A1R-selective agonist PIA (50 nM). A representative experiment is shown (n=3). **B,** DMR experiments in HEK-293T cells expressing CB1R-S452D, together or not with BiP, and incubated with vehicle or WIN-55,212-2 (100 nM). A representative experiment is shown (n=3). **C,** DMR experiments in HEK-293T cells expressing CB1R and incubated with vehicle or WIN-55,212-2 (100 nM) plus U0126 (5 µM) or LY294002 (5 µM). A representative experiment is shown (n=3).

Figure 4. Expression of BiP and CB1R mRNA in the mouse brain

AB, Representative autoradiographic images of coronal sections from adult mouse brain showing the mRNA hybridization pattern of BiP (panel A) and CB1R (panel B). CA, *cornu Ammonis*; DG, dentate gyrus, Str, striatum; Cx, cortex; Cb, cerebellum. **C**, Distribution of CB1R mRNA in the mouse hippocampus. i) Representative dark field image from a section hybridized with ^{33}P-labelled oligonucleotide probes for CB1R mRNA. A positive signal is evident as clusters/accumulation of bright silver grains. Note the moderate signal on the pyramidal cell layer of CA and the very intense signal on scattered cells in the various hippocampal layers. ii, iii) Co-localization of CB1R mRNA and BiP mRNA in cells of the *stratum radiatum* and *stratum lacunosum moleculare* of CA. Pyr, pyramidal cell layer of CA. iv, v) Co-localization of CB1R mRNA and BiP mRNA in cells of the polymorphic layer (Pl). Gr, granular cell layer. Sections were hybridized with ^{33}P-labelled probes for CB1R mRNA (signal visualized as clusters of bright silver grains in dark field images) and with digoxigenin-labelled probes for BiP mRNA (signal visualized as dark precipitate in bright field images). Arrows point to some double-labelled cells. **D,** Quantification of CB1R mRNA-positive cells that co-express BiP mRNA (n=4 mice per group).

Fig 5. Co-localization of BiP mRNA with GAD65/67 or vGlut1 mRNA in the mouse hippocampus

A, Representative mosaic superimages of sections from the adult mouse hippocampus that were hybridized with ^{33}P-labelled probes for BiP mRNA (signal visualized as clusters/accumulation of bright silver grains in the dark field image i) and with a mixture of digoxigenin-labelled probes for GAD65 and GAD67 mRNAs (labelled cells showing dark precipitate in the bright field image ii). Higher magnification images of *cornu Ammonis* (CA; images iii and iv) and dentate gyrus (DG; images v and vi) are shown.

Arrows point to some double-labelled cells, while arrowheads point to some cells that express BiP mRNA but not GAD65/67 mRNA. **B,** Quantification of BiP mRNA-positive cells that co-express GAD65/67 mRNA (n=4 mice per group). **C,** Representative mosaic superimages of sections from the adult mouse hippocampus that were hybridized with ^{33}P-labelled probes for BiP mRNA (signal visualized as clusters/accumulation of bright silver grains in the dark field image i) and with digoxigenin-labelled probes for vGluT1 mRNA (labelled cells showing dark precipitate in the bright field image ii). Higher magnification images of CA (images iii and iv) and DG (images v and vi) are shown. Arrows point to some double-labelled cells, while arrowheads point to some cells that express BiP mRNA but not vGluT1 mRNA. **D,** Quantification of BiP mRNA-positive cells that co-express vGluT1 mRNA (n=4 mice per group).

Figure 6. Subcellular localization of BiP in the mouse brain

A, Western blotting of BiP in total-extract (T), cytosolic (C) and endoplasmic reticulum (ER) fractions from the hippocampus, striatum and cortex of 3-4 month-old WT mice. Calnexin was included as an ER-specific marker. Representative blots from 2 mice are shown. **B,** Quantification of BiP levels in the C and ER fractions relative to BiP levels in the T fraction. $^{**}p<0.01$ from the corresponding ER fraction by one-way ANOVA with Tukey's multiple comparisons test (n=3-4 mice per group). **C,** PLA experiments conducted on synaptosomal fractions isolated from the hippocampus, striatum and cortex of 3-4 month-old CB1R-WT and CB1R-KO mice. Representative images of hippocampal (left column), striatal (mid column) and cortical (right column) synaptosomes, with CB1R-BiP complexes depicted in red, are shown (n=5 mice per group).

Figure 7. CB1R-BiP complexes reside on GABAergic terminals of the mouse hippocampus

A, PLA experiments were conducted on hippocampal sections from 3-4-month-old mice of different genotypes. Representative low-magnification image and selected regions for analysis are shown. Image credit: Allen Institute. In the rest of the panels, CB1R-BiP complexes are shown as red dots, and nuclei are colored in blue by DAPI staining. **B,** Representative images of dentate gyrus (DG) sections from CB1R-floxed, CB1R-KO, GABA-CB1R-KO and Glu-CB1R-KO mice. **C,** Representative images of DG sections from Stop-CB1R, CB1R-RS, GABA-CB1R-RS and Glu-CB1R-RS mice. **D,** Quantification of the number of cells containing one or more dots expressed as the percentage of the total number of cells (DAPI-stained nuclei) in DG sections. $^{**}p<0.01$ from the corresponding CB1R-floxed group or the corresponding CB1R-RS group by one-way ANOVA with Tukey's multiple comparisons test (n=6-7 fields from three different animals per group). **E,** Representative images of CA1 sections from CB1R-floxed, CB1R-KO, GABA-CB1R-KO and Glu-CB1R-KO mice. **F,** Representative images of CA1 sections from Stop-CB1R, CB1R-RS, GABA-CB1R-RS and Glu-CB1R-RS mice. **G,** Quantification of the number of cells containing one or more dots expressed as the percentage of the total number of cells (DAPI-stained nuclei) in CA1 sections. $^{**}p<0.01$ from the corresponding CB1R-floxed group or the corresponding CB1R-RS group by one-way ANOVA with Tukey's multiple comparisons test (n=6-7 fields from three different animals per group).

Figure 8. CB1R-BiP complexes reside on GABAergic terminals of the mouse striatum and cortex

A, PLA experiments were conducted on striatal and cortical sections from 3–4-month-old

mice of different genotypes. Representative low-magnification image and selected regions for analysis are shown. Image credit: Allen Institute. In the rest of the panels, CB1R-BiP complexes are shown as red dots, and nuclei are colored in blue by DAPI staining. **B,** Representative images of striatal sections from CB1R-floxed, CB1R-KO, GABA-CB1R-KO and Glu-CB1R-KO mice. **C,** Representative images of striatal sections from Stop-CB1R, CB1R-RS, GABA-CB1R-RS and Glu-CB1R-RS mice. **D,** Quantification of the number of cells containing one or more dots expressed as the percentage of the total number of cells (DAPI-stained nuclei) in striatal sections. $^{**}p<0.01$ from the corresponding CB1R-floxed group or the corresponding CB1R-RS group by one-way ANOVA with Tukey's multiple comparisons test (n=6-7 fields from three different animals per group). **E,** Representative images of cortical sections from CB1R-floxed, CB1R-KO, GABA-CB1R-KO and Glu-CB1R-KO mice. **F,** Representative images of cortical sections from Stop-CB1R, CB1R-RS, GABA-CB1R-RS and Glu-CB1R-RS mice. **G,** Quantification of the number of cells containing one or more dots expressed as the percentage of the total number of cells (DAPI-stained nuclei) in cortical sections. $^{**}p<0.01$ from the corresponding CB1R-floxed group or the corresponding CB1R-RS group by one-way ANOVA with Tukey's multiple comparisons test (n=6-7 fields from three different animals per group).

Figure 9. BiP does not affect CB1R-evoked hypolocomotion, analgesia, hypothermia and catalepsy *in vivo*

A, Scheme of the experiments. Vehicle or THC (10 mg/kg, 1 i.p. injection per day) was administered for 5 days to 3-4 month-old $BiP^{+/+}$ (BiP-WT) and $BiP^{+/-}$ (BiP-HET) mice. The "cannabinoid tetrad" was evaluated on days 1 and 5, starting 30 min after the corresponding acute-drug injections. **B,** Ambulation (total distance travelled, cm) in the

open-field test on day 1 (left panel) and day 5 (right panel). **C,** Analgesia (latency to pain, s) in the hot-plate test on day 1 (left panel) and day 5 (right panel). **D,** Hypothermia (change in body temperature, °C) as measured with a rectal thermometer on day 1 (left panel) and day 5 (right panel). **E,** Catalepsy (latency to move, s) as measured on a horizontal bar on day 1 (left panel) and day 5 (right panel). In panels B thru E, $^{**}p<0.01$ from the corresponding vehicle group, or $^{\#\#}p<0.01$ from the BiP-WT-vehicle group, by two-way ANOVA with Tukey's multiple comparisons test (panel B, n=18-20 mice per group; panels C, D and E, n=9-10 mice per group).

Figure 10. BiP modulates CB1R-evoked anxiety *in vivo*

Anxiety-like behaviors were measured on an experimental scheme similar to that shown in Fig. 9A. **A,** Anxiety (normalized entries in the center, m^{-1}) in the open-field (OF) test on day 1 (left panel) and day 5 (right panel). Arenas (with their centers outlined in red) illustrating the ambulation of a representative animal per group on day 5 are shown (lower panel). **B,** Anxiety (left panel: number of entries in the open arms; right panel: time spent in the open arms, %) in the elevated plus maze (EPM) test on day 1. In panels A and B, $^{*}p<0.05$, $^{**}p<0.01$ from the corresponding vehicle group, or $^{\#}p<0.05$, $^{\#\#}p<0.01$ from the BiP-WT-vehicle group, by two-way ANOVA with Tukey's multiple comparisons test (panel A, n=18-20 mice per group; panel B, n=22-28 mice per group).

Table legends

Table 1. Oligonucleotides used for *in situ* hybridization histochemistry

Table 2. Effect of CB1R-CTD phosphomimetic mutants on CB1R-BiP interaction

Scheme of the Y2H experiment using every possible single phosphomimetic mutant (S/T→D) within CB1R-CTD as bait, and BiP-IR as prey. Only one clone abrogated the interaction (CB1R-CTD-S452D).

Table 1. Oligonucleotides used for *in situ* hybridization histochemistry

Oligonucleotide designation	mRNA	Accession number	bp limits	Oligonucleotide sequence
mCB1/1	Cannabinoid receptor 1	U22948.1	186-230	GATGGTACGGAAGGTGGTATCTGCAAGGCCGTCTAAGATCGACTT
mCB1/2	Cannabinoid receptor 1	U22948.1	556-600	ATAGCACCAGCAGGTTCTCCAGAACCGTGAAGGTGCCCAGGGTGA
mCB1/3	Cannabinoid receptor 1	U22948.1	1556-1601	CAGAGCCTCGGCAGACGTGTCTGTGGACACAGACATGGTCACCTT
mGRP78/1	78 kDa glucose-regulated protein (BiP)	D78645.1	121-165	TCTTGTCCTCCTCCTCGGCCCGCACCGCGCCCAGCAGCAGCAACG
mGRP78/2	78 kDa glucose-regulated protein (BiP)	D78645.1	1262-1306	ACACCAGCCTGGACAGCGGCACCATAGGCTACAGCCTCATCGGGG
mGRP78/3	78 kDa glucose-regulated protein (BiP)	D78645.1	1996-2040	ATGTATCCTCTTCACCAGTTGGGGGAGGGCCTCCACTTCCATAGA
rmGAD65/1	Glutamic acid decarboxylase 65	NM_008078.2	421-465	CTTGTTTCCGATGCCGCCCGTGAACTTTTGGGCCACCTGGCACCA
rmGAD65/2	Glutamic acid decarboxylase 65	NM_008078.2	776-820	GCGTCAAAATTTCCTCCAGATTTTGCGGTTGGTCTGCCAATTCCC
rGAD/5	Glutamic acid decarboxylase 67	M76177.1	1601-1654	ATAGAGGTATTCAGCCAGCTCCAGGCATTTGTTGATCTGATTTTCAAATCCCAC
rVGluT1/1	Vesicular GluT1 Transporter	NM_053859.1	127-171	CAGGGCGCGCCCCGCCAGCTTCCGAAACTCCTCCTGCCGGAACTC
rVGluT1/2	Vesicular GluT1 Transporter	NM_053859.1	1756-1800	GTCCCGGACAGGGGGTGGGGGCCTTGGAGGCTGAACTGTGCTGTG

Table 2. Effect of CB1R-CTD phosphomimetic mutants on CB1R-BiP interaction

Scheme of the Y2H experiment using every possible single phosphomimetic mutant (S/T→D) within CB1R-CTD as bait, and BiP-IR as prey. Only one clone abrogated the interaction (CB1R-CTD-S452D).

Bait plasmid	Prey plasmid	Interaction
pGBT9 CB1R-CTD-S410D	pACT2 BiP-IR	+ (n=3)
pGBT9 CB1R-CTD-S414D	pACT2 BiP-IR	+ (n=3)
pGBT9 CB1R-CTD-T418D	pACT2 BiP-IR	+ (n=3)
pGBT9 CB1R-CTD-S425D	pACT2 BiP-IR	+ (n=3)
pGBT9 CB1R-CTD-S429D	pACT2 BiP-IR	+ (n=3)
pGBT9 CB1R-CTD-S441D	pACT2 BiP-IR	+ (n=3)
pGBT9 CB1R-CTD-S448D	pACT2 BiP-IR	+ (n=3)
pGBT9 CB1R-CTD-S452D	pACT2 BiP-IR	– (n=3)
pGBT9 CB1R-CTD-T453D	pACT2 BiP-IR	+ (n=3)
pGBT9 CB1R-CTD-T460D	pACT2 BiP-IR	+ (n=3)
pGBT9 CB1R-CTD-S462D	pACT2 BiP-IR	+ (n=3)
pGBT9 CB1R-CTD-S464D	pACT2 BiP-IR	+ (n=3)
pGBT9 CB1R-CTD-T465D	pACT2 BiP-IR	+ (n=3)
pGBT9 CB1R-CTD-T467D	pACT2 BiP-IR	+ (n=3)
pGBT9 CB1R-CTD-S468D	pACT2 BiP-IR	+ (n=3)

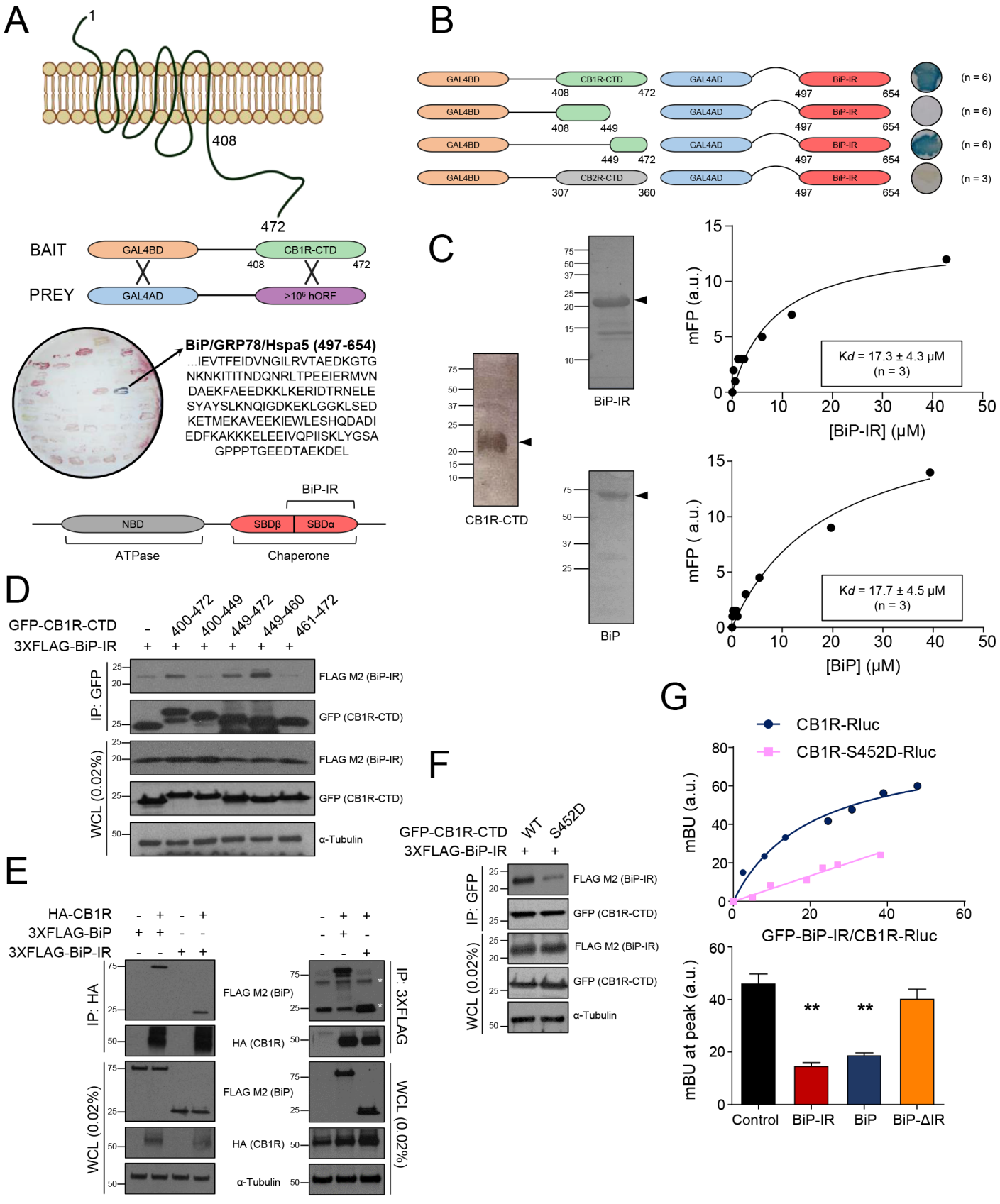
A
1
408
472
BAIT
GAL4BD
CB1R-CTD
408
472
PREY
GAL4AD
>10⁶ hORF
BiP/GRP78/Hspa5 (497-654)
...IEVTFEIDVNGILRVTAEDKGTG
NKNKITITNDQNRLTPEEIERMVN
DAEKFAEEDKKLKERIDTRNELE
SYAYSLKNQIGDKEKLGGKLSED
KETMEKAVEEKIEWLESHQDADI
EDFKAKKKELEEIVQPIISKLYGSA
GPPPTGEEDTAEKDEL
BiP-IR
NBD
SBDβ
SBDα
ATPase
Chaperone
B
GAL4BD
CB1R-CTD
408
472
GAL4AD
BiP-IR
497
654
(n = 6)
GAL4BD
408
449
GAL4AD
BiP-IR
497
654
(n = 6)
GAL4BD
449
472
GAL4AD
BiP-IR
497
654
(n = 6)
GAL4BD
CB2R-CTD
307
360
GAL4AD
BiP-IR
497
654
(n = 3)
C
CB1R-CTD
BiP-IR
BiP
mFP (a.u.)
[BiP-IR] (μM)
Kd = 17.3 ± 4.3 μM
(n = 3)
mFP (a.u.)
[BiP] (μM)
Kd = 17.7 ± 4.5 μM
(n = 3)
D
GFP-CB1R-CTD
3XFLAG-BiP-IR
400-472
400-449
449-472
449-460
461-472
IP: GFP
WCL (0.02%)
FLAG M2 (BiP-IR)
GFP (CB1R-CTD)
α-Tubulin
E
HA-CB1R
3XFLAG-BiP
3XFLAG-BiP-IR
IP: HA
WCL (0.02%)
FLAG M2 (BiP)
HA (CB1R)
α-Tubulin
IP: 3XFLAG
F
GFP-CB1R-CTD
WT
S452D
3XFLAG-BiP-IR
IP: GFP
WCL (0.02%)
FLAG M2 (BiP-IR)
GFP (CB1R-CTD)
α-Tubulin
G
CB1R-Rluc
CB1R-S452D-Rluc
mBU (a.u.)
GFP-BiP-IR/CB1R-Rluc
mBU at peak (a.u.)
**
**
Control
BiP-IR
BiP
BiP-ΔIR

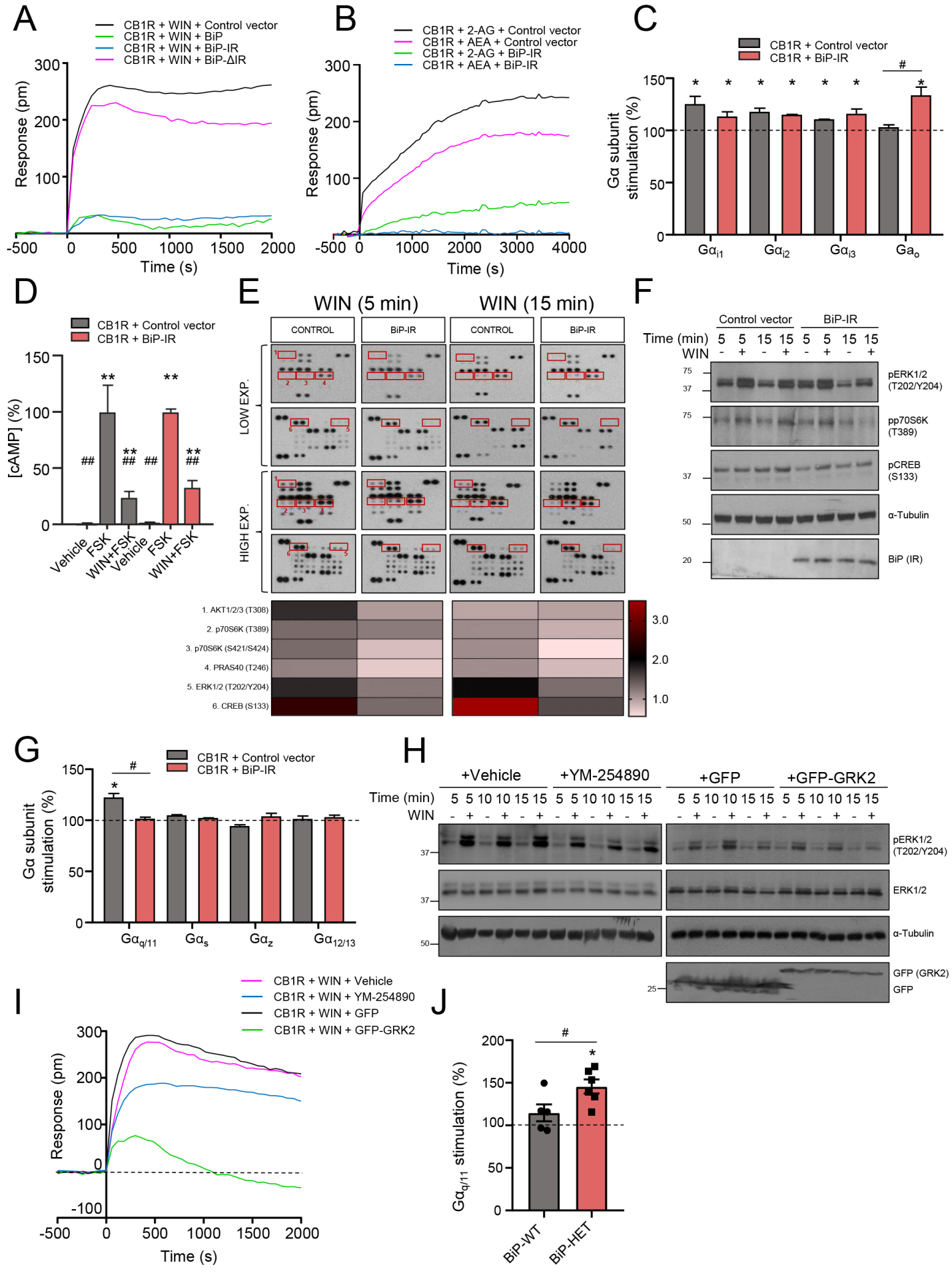
A
CB1R + WIN + Control vector
CB1R + WIN + BiP
CB1R + WIN + BiP-IR
CB1R + WIN + BiP-ΔIR
Response (pm)
Time (s)
B
CB1R + 2-AG + Control vector
CB1R + AEA + Control vector
CB1R + 2-AG + BiP-IR
CB1R + AEA + BiP-IR
Response (pm)
Time (s)
C
CB1R + Control vector
CB1R + BiP-IR
Gα subunit stimulation (%)
Gαi1
Gαi2
Gαi3
Gao
D
CB1R + Control vector
CB1R + BiP-IR
[cAMP] (%)
Vehicle
FSK
WIN+FSK
Vehicle
FSK
WIN+FSK
E
WIN (5 min)
WIN (15 min)
CONTROL
BiP-IR
CONTROL
BiP-IR
LOW EXP.
HIGH EXP.
1. AKT1/2/3 (T308)
2. p70S6K (T389)
3. p70S6K (S421/S424)
4. PRAS40 (T246)
5. ERK1/2 (T202/Y204)
6. CREB (S133)
F
Control vector
BiP-IR
Time (min)
WIN
pERK1/2 (T202/Y204)
pp70S6K (T389)
pCREB (S133)
α-Tubulin
BiP (IR)
G
CB1R + Control vector
CB1R + BiP-IR
Gα subunit stimulation (%)
Gαq/11
Gαs
Gαz
Gα12/13
H
+Vehicle
+YM-254890
+GFP
+GFP-GRK2
Time (min)
WIN
pERK1/2 (T202/Y204)
ERK1/2
α-Tubulin
GFP (GRK2)
GFP
I
CB1R + WIN + Vehicle
CB1R + WIN + YM-254890
CB1R + WIN + GFP
CB1R + WIN + GFP-GRK2
Response (pm)
Time (s)
J
Gαq/11 stimulation (%)
BiP-WT
BiP-HET

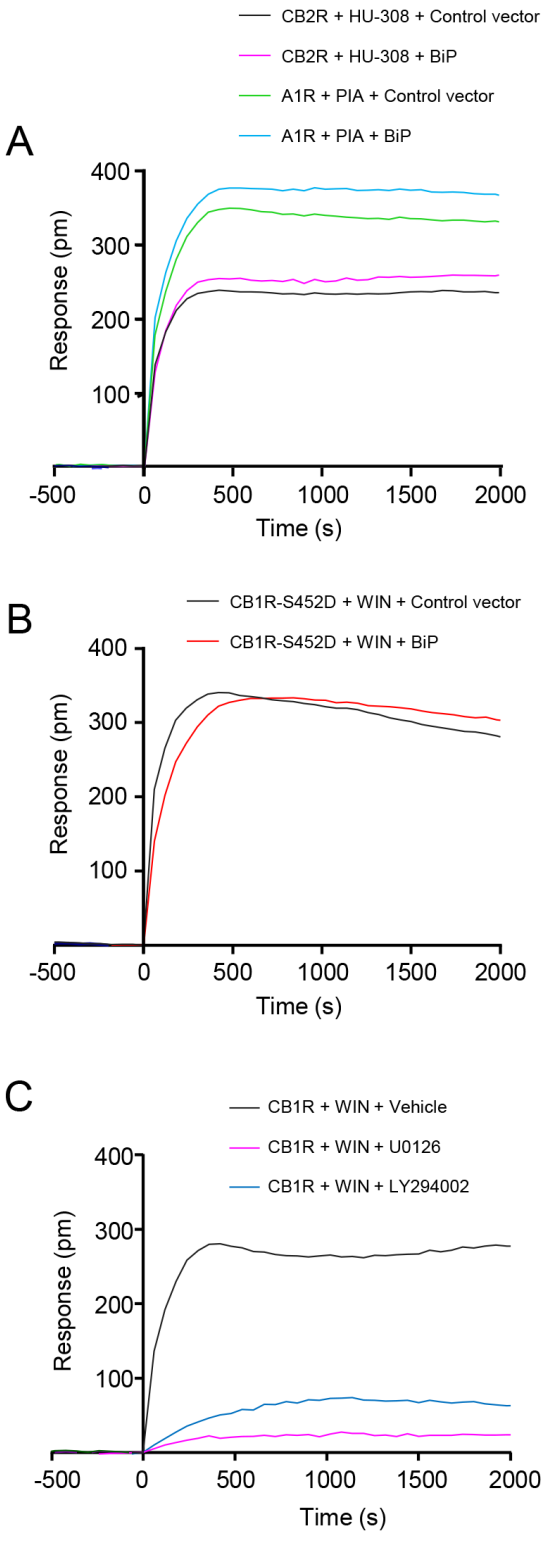
A
CB2R + HU-308 + Control vector
CB2R + HU-308 + BiP
A1R + PIA + Control vector
A1R + PIA + BiP
Response (pm)
400
300
200
100
-500
0
500
1000
1500
2000
Time (s)
B
CB1R-S452D + WIN + Control vector
CB1R-S452D + WIN + BiP
Response (pm)
400
300
200
100
-500
0
500
1000
1500
2000
Time (s)
C
CB1R + WIN + Vehicle
CB1R + WIN + U0126
CB1R + WIN + LY294002
Response (pm)
400
300
200
100
-500
0
500
1000
1500
2000
Time (s)

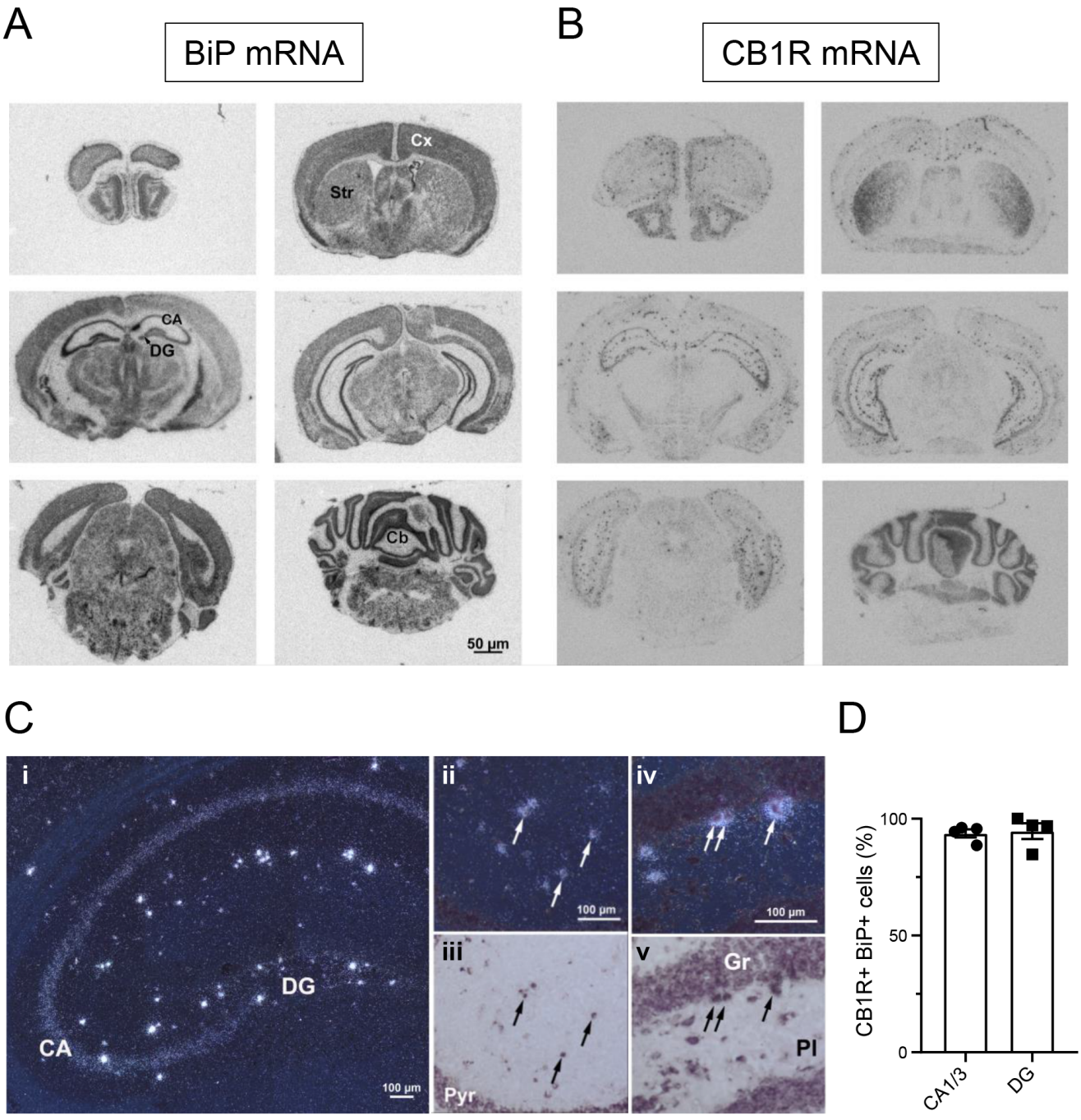
A
BiP mRNA
B
CB1R mRNA
Cx
Str
CA
DG
Cb
50 µm
C
i
DG
CA
100 µm
ii
100 µm
iv
100 µm
iii
Pyr
v
Gr
Pl
D
CB1R+ BiP+ cells (%)
100
50
0
CA1/3
DG

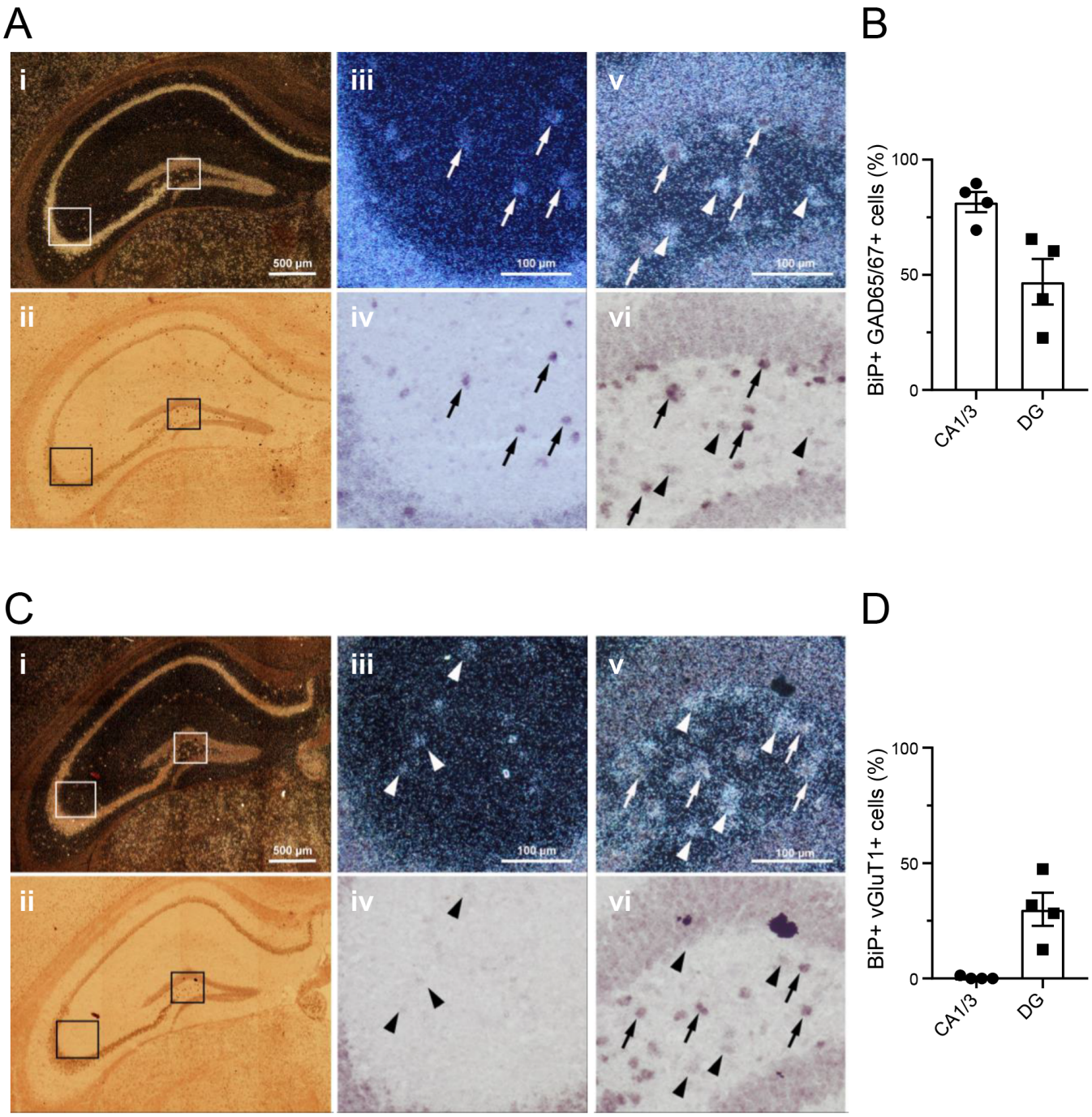
A
i
iii
v
ii
iv
vi
500 µm
100 µm
100 µm
500 µm
100 µm
100 µm
B
BiP+ GAD65/67+ cells (%)
100
50
0
CA1/3
DG
C
i
iii
v
ii
iv
vi
500 µm
100 µm
100 µm
D
BiP+ vGluT1+ cells (%)
100
50
0
CA1/3
DG

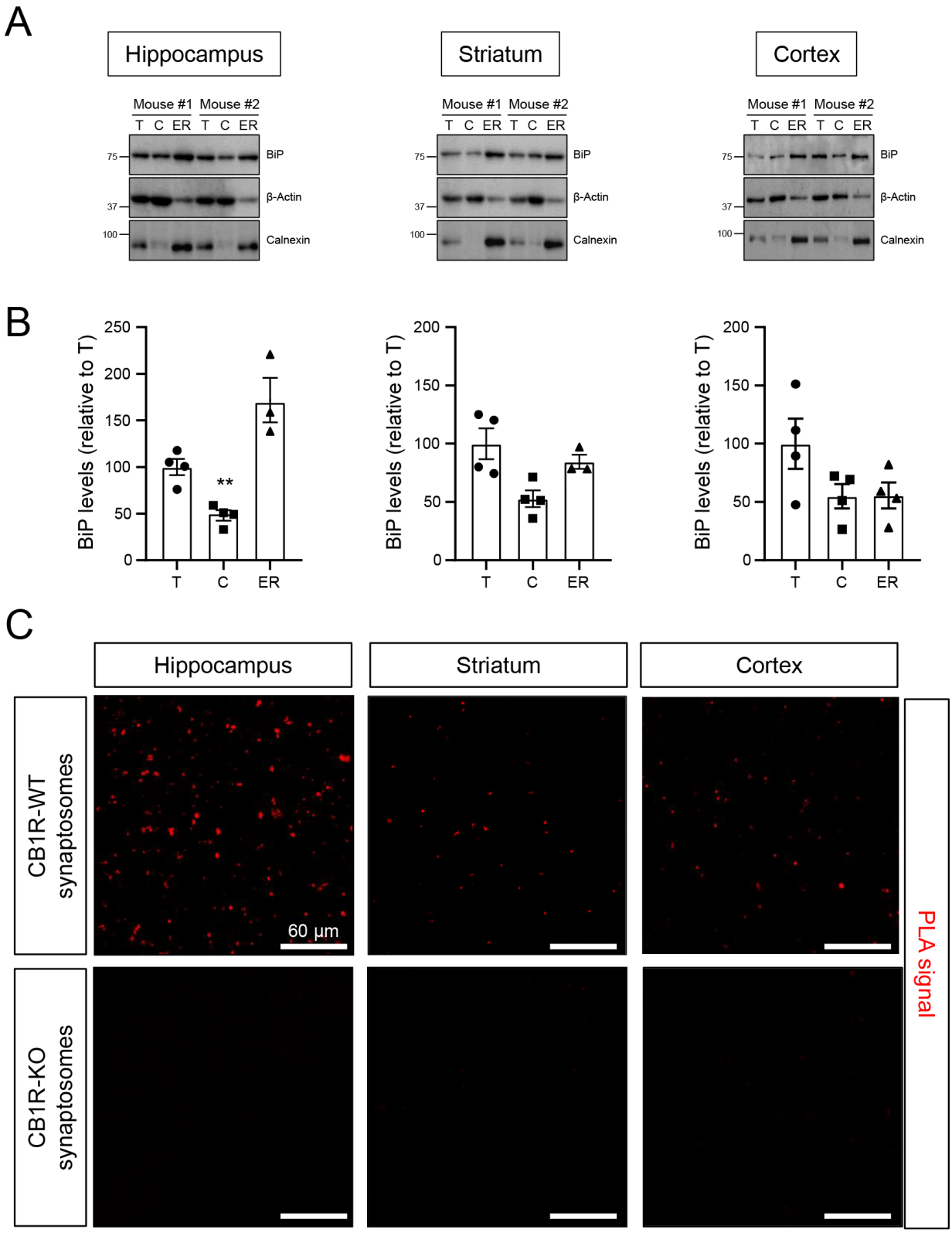
A
Hippocampus
Striatum
Cortex
Mouse #1
Mouse #2
T C ER T C ER
75
37
100
BiP
β-Actin
Calnexin
B
BiP levels (relative to T)
250
200
150
100
50
0
**
T
C
ER
C
CB1R-WT synaptosomes
CB1R-KO synaptosomes
60 µm
PLA signal

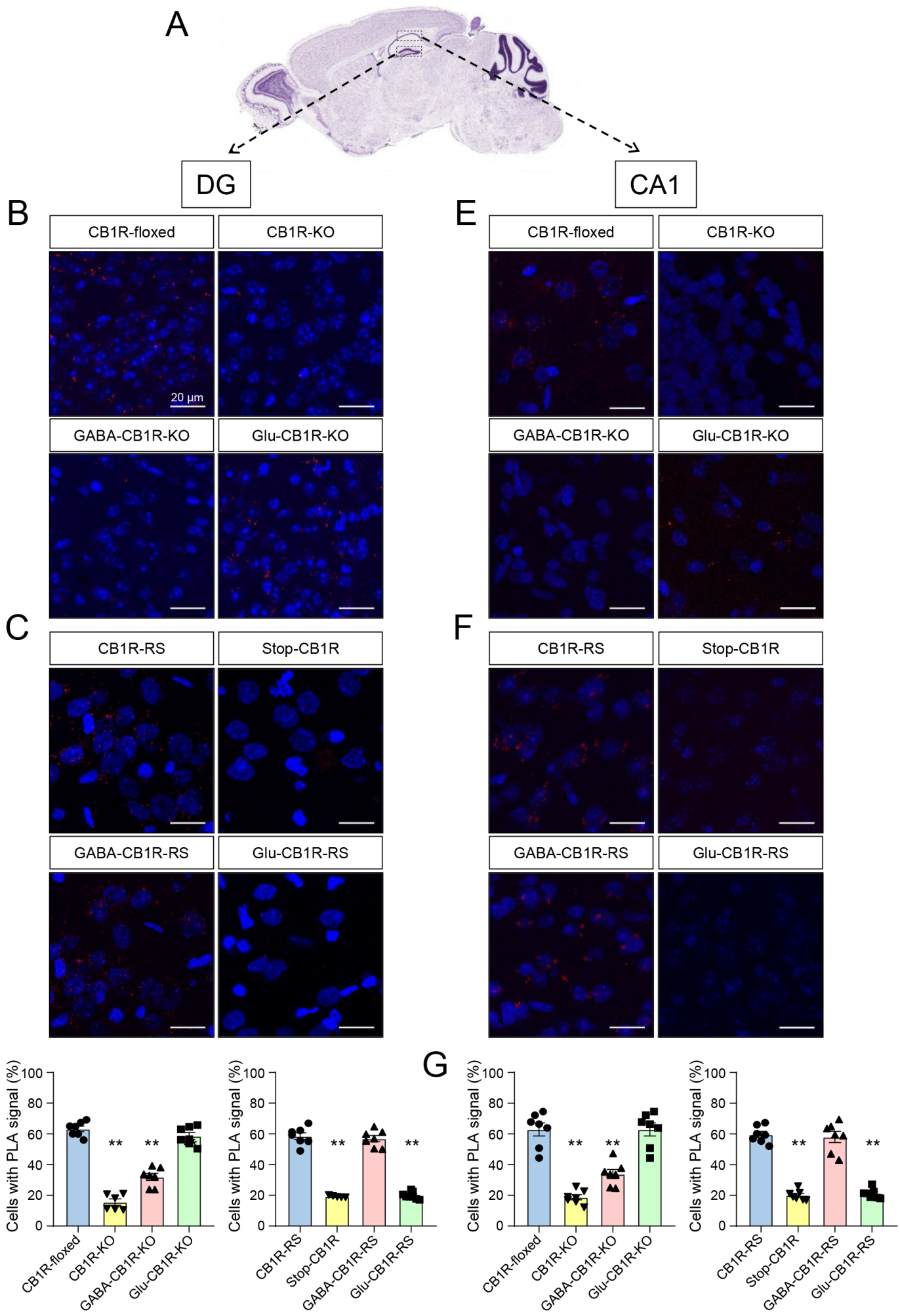
A
DG
CA1
B
CB1R-floxed
CB1R-KO
20 μm
GABA-CB1R-KO
Glu-CB1R-KO
E
CB1R-floxed
CB1R-KO
GABA-CB1R-KO
Glu-CB1R-KO
C
CB1R-RS
Stop-CB1R
GABA-CB1R-RS
Glu-CB1R-RS
F
CB1R-RS
Stop-CB1R
GABA-CB1R-RS
Glu-CB1R-RS
D
Cells with PLA signal (%)
0
20
40
60
80
100
**
**
CB1R-floxed
CB1R-KO
GABA-CB1R-KO
Glu-CB1R-KO
Cells with PLA signal (%)
0
20
40
60
80
100
**
**
CB1R-RS
Stop-CB1R
GABA-CB1R-RS
Glu-CB1R-RS
G
Cells with PLA signal (%)
0
20
40
60
80
100
**
**
CB1R-floxed
CB1R-KO
GABA-CB1R-KO
Glu-CB1R-KO
Cells with PLA signal (%)
0
20
40
60
80
100
**
**
CB1R-RS
Stop-CB1R
GABA-CB1R-RS
Glu-CB1R-RS

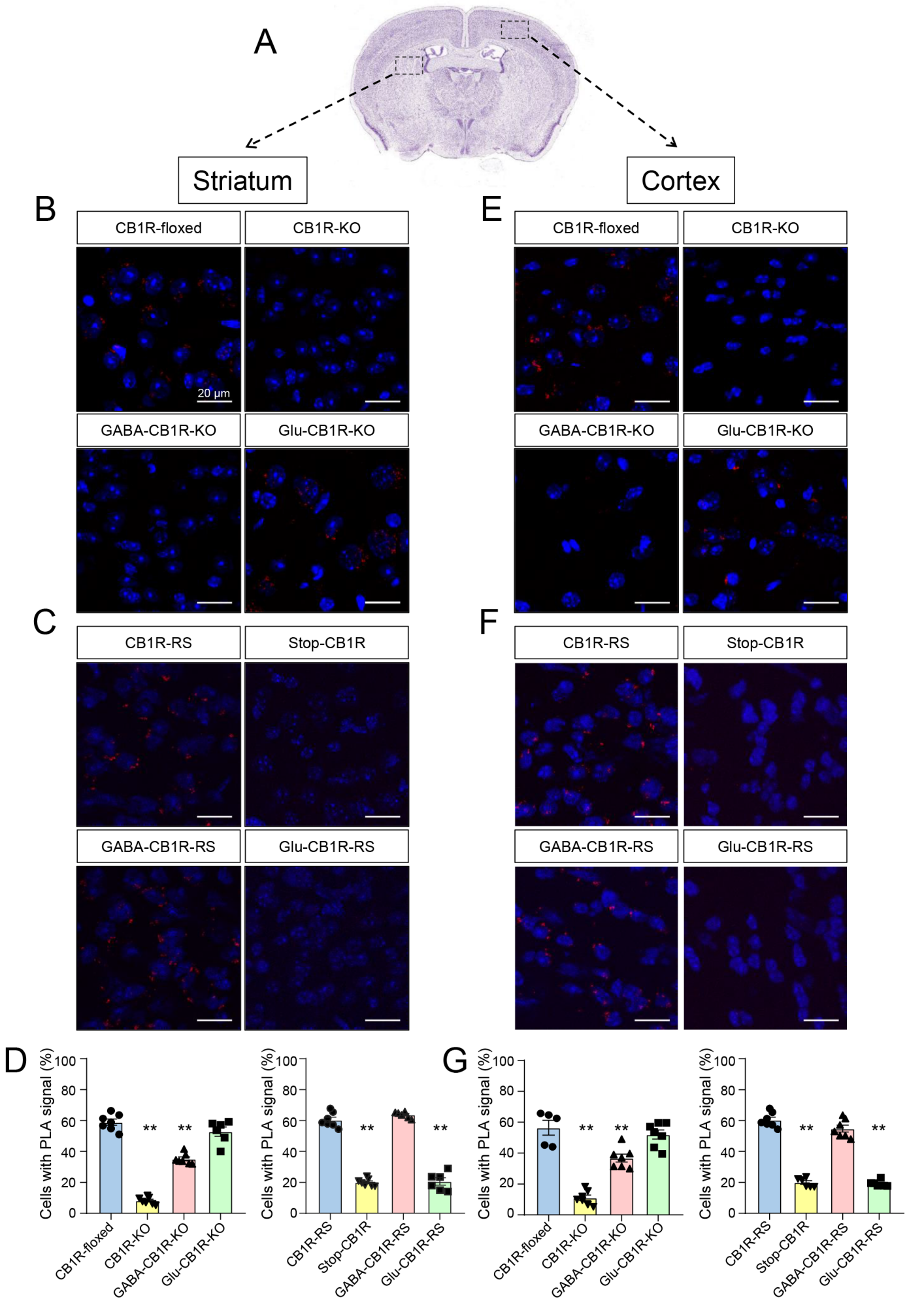
A
Striatum
Cortex
B
CB1R-floxed
CB1R-KO
20 μm
GABA-CB1R-KO
Glu-CB1R-KO
E
CB1R-floxed
CB1R-KO
GABA-CB1R-KO
Glu-CB1R-KO
C
CB1R-RS
Stop-CB1R
GABA-CB1R-RS
Glu-CB1R-RS
F
CB1R-RS
Stop-CB1R
GABA-CB1R-RS
Glu-CB1R-RS
D
Cells with PLA signal (%)
0
20
40
60
80
100
**
**
CB1R-floxed
CB1R-KO
GABA-CB1R-KO
Glu-CB1R-KO
Cells with PLA signal (%)
0
20
40
60
80
100
**
**
CB1R-RS
Stop-CB1R
GABA-CB1R-RS
Glu-CB1R-RS
G
Cells with PLA signal (%)
0
20
40
60
80
100
**
**
CB1R-floxed
CB1R-KO
GABA-CB1R-KO
Glu-CB1R-KO
Cells with PLA signal (%)
0
20
40
60
80
100
**
**
CB1R-RS
Stop-CB1R
GABA-CB1R-RS
Glu-CB1R-RS

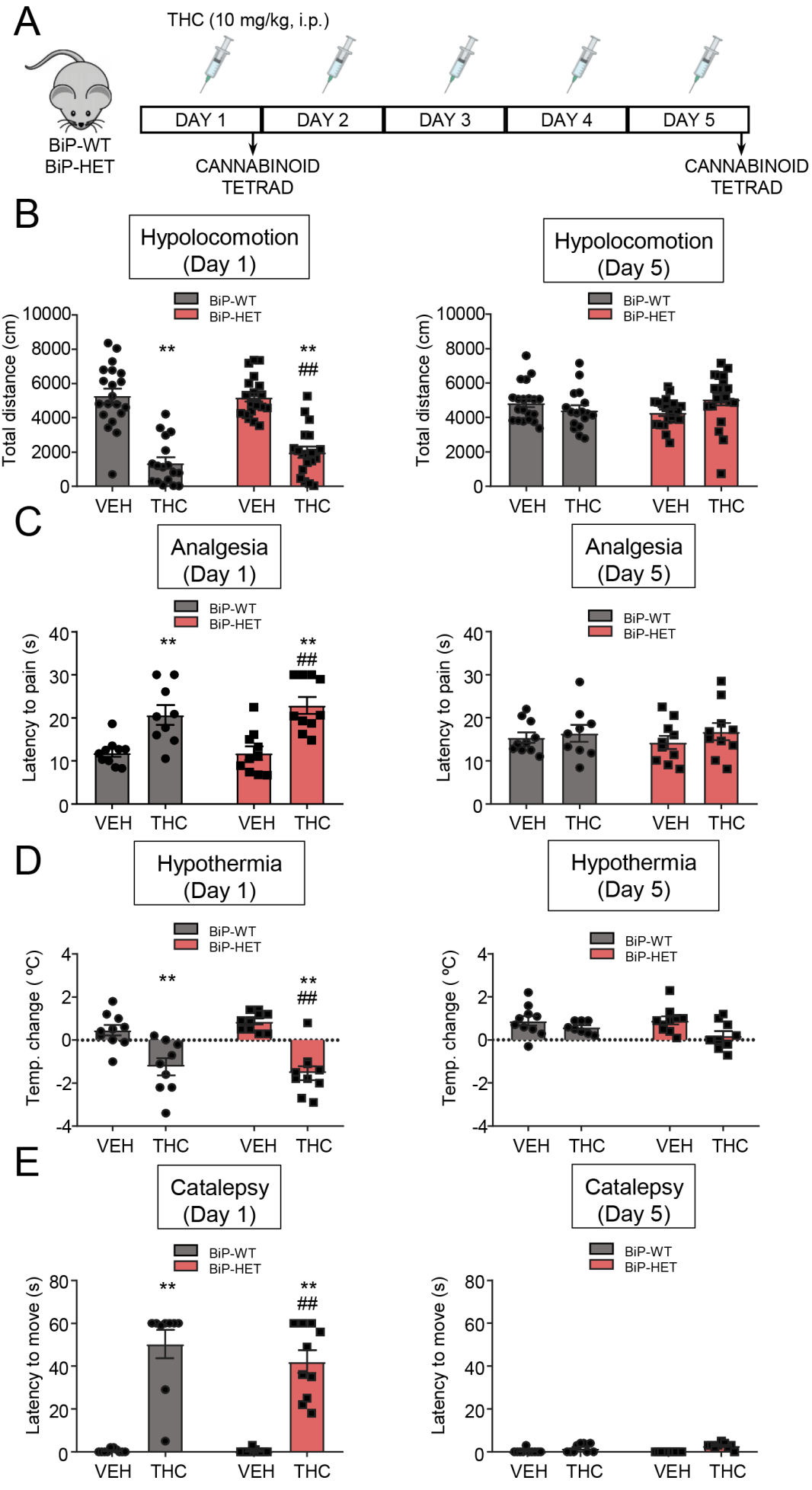
A
THC (10 mg/kg, i.p.)
DAY 1
DAY 2
DAY 3
DAY 4
DAY 5
BiP-WT
BiP-HET
CANNABINOID TETRAD
CANNABINOID TETRAD
B
Hypolocomotion (Day 1)
Hypolocomotion (Day 5)
Total distance (cm)
BiP-WT
BiP-HET
VEH
THC
C
Analgesia (Day 1)
Analgesia (Day 5)
Latency to pain (s)
D
Hypothermia (Day 1)
Hypothermia (Day 5)
Temp. change (ºC)
E
Catalepsy (Day 1)
Catalepsy (Day 5)
Latency to move (s)

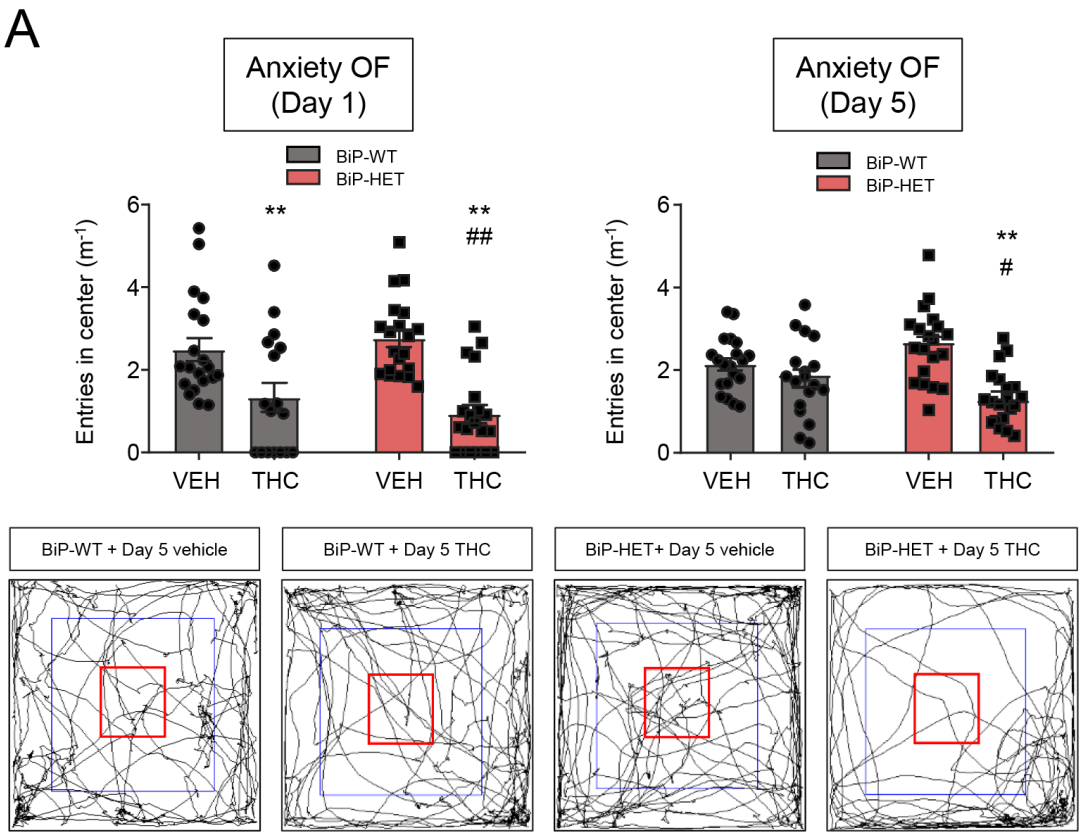
A
Anxiety OF (Day 1)
Anxiety OF (Day 5)
BiP-WT
BiP-HET
Entries in center (m-1)
VEH
THC
BiP-WT + Day 5 vehicle
BiP-WT + Day 5 THC
BiP-HET+ Day 5 vehicle
BiP-HET + Day 5 THC

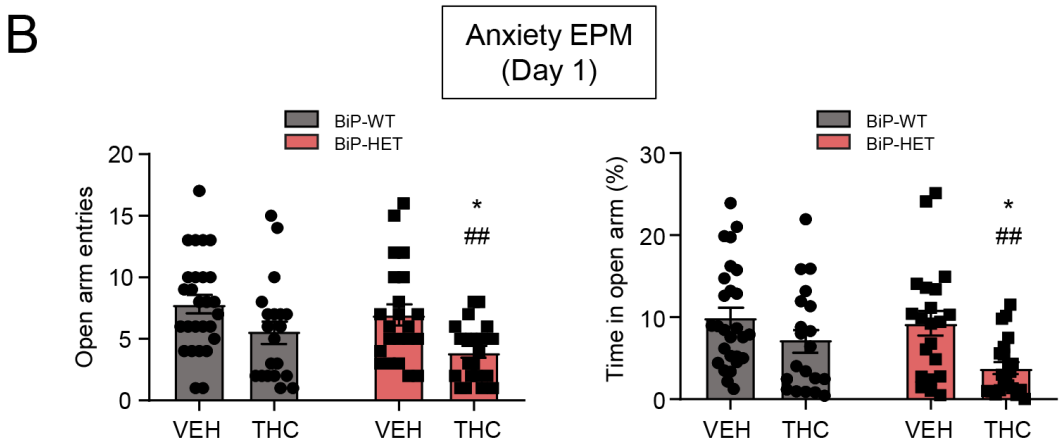
B
Anxiety EPM (Day 1)
BiP-WT
BiP-HET
Open arm entries
Time in open arm (%)
VEH
THC